UNCLASSIFIED

~~CONFIDENTIAL~~

UD

NASA TM X-1158

NASA TECHNICAL MEMORANDUM

NASA TM X-1158

AERODYNAMIC CHARACTERISTICS OF A MANNED LIFTING ENTRY VEHICLE WITH MODIFIED TIP FINS AT MACH 6.8

by Charles L. Ladson

Langley Research Center

Langley Station, Hampton, Va.

NATIONAL AERONAUTICS AND SPACE ADMINISTRATION • WASHINGTON, D. C. • OCTOBER 1965

~~CONFIDENTIAL~~

UNCLASSIFIED

NASA TM X-1158

AERODYNAMIC CHARACTERISTICS OF A MANNED LIFTING ENTRY VEHICLE WITH MODIFIED TIP FINS AT MACH 6.8

By Charles L. Ladson

Langley Research Center
Langley Station, Hampton, Va.

NATIONAL AERONAUTICS AND SPACE ADMINISTRATION

AERODYNAMIC CHARACTERISTICS OF A MANNED LIFTING ENTRY VEHICLE WITH MODIFIED TIP FINS AT MACH 6.8*

By Charles L. Ladson
Langley Research Center

SUMMARY

The effects of modifications of the tip fins and center fin on the aerodynamic characteristics of a model of a manned lifting entry vehicle with negative camber, a flat bottom, a blunt leading edge, and a delta planform (designated HL-10) have been determined at a Mach number of 6.8. The configuration with modified tip and center fins was directionally and laterally stable throughout the test angle-of-attack range. The maximum trimmed lift coefficient obtained was 0.48 and the maximum trimmed lift-drag ratio was about 1.14. Roll control effectiveness increased with increasing angle of attack and with increasing positive elevon deflection angle. The yawing moment due to roll control was very small.

Newtonian theory generally predicts the trends in incremental directional and lateral stability of tip fins due to fin toe-in and roll-out angles, but does not give close estimates of the magnitudes. Simple Newtonian theory does not predict the incremental pitching moment due to elevon deflection because of the complex flow field over the elevons at both positive and negative deflection angles.

INTRODUCTION

An investigation to determine the aerodynamic characteristics, problems, and possible solutions to the problems of a manned lifting entry vehicle having a maximum hypersonic lift-drag ratio of about 1 has been underway at the Langley Research Center since early 1962. As a result of preliminary studies, a configuration with negative camber, a flat bottom, a blunt leading edge, and a delta planform, designated HL-10, was selected for testing throughout the Mach number range. Some of the data previously obtained are published in references 1 to 16. Results in reference 3 indicated that the basic body shape in combination with a trapezoidal center fin and triangular-planform tip fins (designated center fin E and tip fin D in ref. 3) seemed to be a promising configuration for further investigation at transonic and supersonic speeds.

*Title, Unclassified.

The results from tests of this configuration at transonic Mach numbers between 0.2 and 1.2 are presented in reference 5 and, within the limits of the test conditions, no large problem areas are evident. At supersonic speeds, however, directional instability occurs within the angle-of-attack range from about 20° to 30° at Mach numbers between 1.5 and 3.0. (See refs. 6 and 7.) It is in this angle-of-attack range that the maximum trimmed lift-drag ratio occurs; thus it is important to eliminate the instability in this range. The supersonic data also show that both the tip fins and the center fin are effective at the lower Mach numbers and angles of attack but only the tip fins are effective at the higher Mach numbers and angles of attack. Thus, modifications to both tip fins and the center fin are considered in the present investigation in an effort to achieve a directionally stable vehicle.

Variations in both center- and tip-fin geometry are incorporated on the basic configuration and tested at supersonic speeds. The more promising configurations are also tested at $M = 6.8$ in the Langley 11-inch hypersonic tunnel to determine the aerodynamic characteristics at this high speed. Included in the hypersonic tests are variations in tip-fin roll-out angle and toe-in angle for a fin of larger planform area than that presented in reference 3.

The purpose of the present report is to present the longitudinal, directional, and lateral stability characteristics, and the longitudinal and lateral control characteristics of the HL-10 configuration with these fin modifications. The data are obtained at angles of attack up to about 50° at a Reynolds number based on model length of about 1.7×10^6. Several of the aerodynamic parameters, including the incremental directional and lateral stability of the fins, are compared with Newtonian theory.

SYMBOLS

Measurements for this investigation were taken in the U.S. Customary System of Units. Equivalent values are indicated herein parenthetically in the International System (SI) in the interest of promoting use of this system in future NASA reports. Details concerning the use of SI, together with physical constants and conversion factors, are given in reference 17.

b span, in. (cm)

C_A axial-force coefficient, $\frac{\text{Axial force}}{qS}$

C_D drag coefficient, $\frac{\text{Drag}}{qS}$

C_L lift coefficient, $\frac{\text{Lift}}{qS}$

C_l rolling-moment coefficient, $\frac{\text{Rolling moment}}{qSb}$

$C_{l_\beta} = \frac{\partial C_l}{\partial \beta}$ per degree

C_m pitching-moment coefficient, $\frac{\text{Pitching moment}}{qSl}$

C_N normal-force coefficient, $\frac{\text{Normal force}}{qS}$

C_n yawing-moment coefficient, $\frac{\text{Yawing moment}}{qSb}$

$C_{n_\beta} = \frac{\partial C_n}{\partial \beta}$ per degree

C_p pressure coefficient

C_Y side-force coefficient, $\frac{\text{Side force}}{qS}$

$C_{Y_\beta} = \frac{\partial C_Y}{\partial \beta}$ per degree

L/D lift-drag ratio

l body length, in. (cm)

M free-stream Mach number

q free-stream dynamic pressure, lbf/sq ft (N/m^2)

R Reynolds number based on body length l

S reference area equal to projected planform area with elevons, sq in. (sq cm)

S_F reference area of tip fin, sq in. (sq cm)

X,Y,Z body axes

x,y,z distances along body axes, in. (cm)

x_F, y_F, z_F distances along body axes between model center of moments and tip-fin center of pressure; positive for tip-fin center of pressure behind and above model moment center

α angle of attack, deg

β angle of sideslip, deg

δ_a aileron deflection angle, equal to right-elevon deflection angle minus left-elevon deflection angle, deg

δ_e elevon deflection angle; angle between elevon surface and model surface ahead of elevon measured in plane normal to elevon hinge line; positive for trailing edge down; (both upper and lower surface elevons move for positive and negative deflections), deg

ϵ fin toe-in angle; angle between model vertical plane of symmetry and fin outer surface measured in horizontal reference plane of model (see fig. 1(c)), deg

ϵ' fin toe-in angle; angle between model vertical plane of symmetry and fin outer surface measured in plane of body lower surface (see fig. 1(c)), deg

ϕ fin roll-out angle; angle between model vertical plane of symmetry and fin outer surface measured in plane normal to fin roll axis (see fig. 1(c)), deg

ϕ' fin roll-out angle; angle between model vertical plane of symmetry and fin outer surface measured in vertical cutting plane which is normal to fin outer surface (see fig. 1(c)), deg

Subscript:

max maximum

MODEL AND DESIGNATIONS

Three-view drawings showing details of the HL-10 configuration in combination with the fins tested are presented in figure 1. Photographs of the 8-inch (20.32-cm) model are shown in figure 2. Each of the tip dorsal fins designated I has an area of 8.9 percent of the model planform area. The center fin, designated fin E_2, has a planform area of 9.9 percent of the model planform area. These fin designations are a continuation of those presented in reference 3, and details of fins D and E may be found in this reference. Three combinations of tip-fin roll-out and toe-in angles were investigated using the I fin planform shape. The various combinations are identified by subscripts on the fin designation and are as follows:

Fin	ϵ, deg	ϵ', deg	ϕ, deg	ϕ', deg
I_4	11.0	13.7	8.5	11.5
I_5	5.8	10.4	15.0	17.5
I_6	12.0	16.6	15.0	19.3

The values of fin toe-in and roll-out angles are not theoretically derived; they were measured from existing models and thus there may be slight errors. Tip fin I_4 has been previously designated as $I_{8.5(13)}$, the subscripts indicating the design roll-out and toe-in angles. This cumbersome designation has been replaced by the designation I_4. Cross-section ordinates for the basic body without tip fins are presented in reference 5.

The model shown in figure 2 was constructed of stainless steel and was equipped with interchangeable fins and elevons. As mentioned in reference 3, the model caused a tunnel blockage problem at angles of attack above about 40° for an elevon deflection angle of 0°. For positive elevon deflection angles, the maximum angle of attack at which tunnel blockage occurred was reduced. A 6-inch (15.24-cm) model was constructed, therefore, in order to obtain data at higher angles of attack. This model, which was made of aluminum, provided for the balance support to enter through the upper surface rather than through the base in an effort to reduce the support interference at high angles of attack. (See schlieren photographs, figs. 3(d) to 3(g).) The 6-inch (15.24-cm) model was not tested with the center vertical tail or the upper surface center-line cylindrical fairing because of the type of balance support used. Data in reference 3 show that the center tail is shielded from the flow and it produces no aerodynamic inputs at angles of attack above about 20°; therefore, data on the 6-inch (15.24-cm) model should be representative.

All coefficients are based on the total projected planform area, the span, and the length of the model. The moment center for both models is located at 53 percent of the body length behind the nose and at 1.25 percent of the body length below the reference center line. The reference areas and lengths are as follows:

S,		b,		l,	
sq in.	(sq cm)	in.	(cm)	in.	(cm)
22.84	147.35	5.155	13.094	8.000	20.32
12.85	82.90	3.866	9.820	6.000	15.24

APPARATUS, TESTS, AND PROCEDURE

The data contained herein were obtained in the Mach 6.8 test section of the Langley 11-inch hypersonic tunnel. A description and calibration of this facility is presented in reference 18. Tests on the 8-inch (20.32-cm) model were conducted at an average stagnation pressure of about 20 atmospheres absolute (2.026 MN/m^2) at an average Mach number of about 6.87. For the 6-inch (15.24-cm) model, the stagnation pressure was about 25 atmospheres (2.533 MN/m^2), and the average Mach number was about 6.88. All tests were conducted at a stagnation temperature of about 600° F (589° K). For both models, the Reynolds number based on model length was about 1.7×10^6.

The angles of attack and sideslip of the model were measured optically by use of a light beam reflected onto a calibrated scale from a prism imbedded within the model surface. This method gave the true angle of attack of the model, including the deflection of the model and sting under load. The model base pressure for all tests was measured on the 8-inch (20.32-cm) model. The contribution of base pressure to axial force was found to be negligible compared with the measured axial force; thus, the data presented are uncorrected. Six-component, electrical strain-gage balances were used to obtain the force and moment data.

All lateral- and directional-stability data were obtained at five angles of sideslip between 0° and 8°. Inasmuch as the directional and lateral data were linear with β, only the slopes have been presented. All longitudinal performance data are referred to the stability axis system, whereas the directional-, lateral-, and longitudinal-stability results are referred to the body axis system.

ACCURACY OF RESULTS

The accuracy for the angles of attack and sideslip was ±0.2°. A summary of the average values and accuracies for Mach number and dynamic pressure and of the balance accuracies in terms of the aerodynamic coefficients is presented in the following table:

α, deg	M	q,		Accuracy of static balance calibrations in terms of -					
		lbf/sq ft abs	kN/m^2	C_N	C_A	C_m	C_l	C_n	C_Y
0 to 40	6.87 ± 0.03	376 ± 1.3	18 ± 0.06	0.0026	0.0012	0.0003	0.0001	0.0002	0.0008
32 to 50	6.88 ± 0.03	472 ± 1.3	23 ± 0.06	.0059	.0059	.0006	.0002	.0002	.0006

The Mach number varied about ±0.03 and the dynamic pressure varied about 6 lbf/sq ft (287 N/m^2) during each test as a result of a change in tunnel throat size due to heating as the test progressed. These variations were accounted for in the data reduction.

RESULTS

Longitudinal Characteristics

The longitudinal characteristics of the configuration with tip fins I_5 and I_6 are presented in figure 4. These fins have the same roll-out angle (ϕ = 15°) but they differ in toe-in angle (ϵ = 5.8° and ϵ = 12.0°, respectively). Comparison of figures 4(a) and 4(b) shows that increasing the toe-in angle from 5.8° to 12.0° increases both the lift and the drag coefficients slightly, with little effect on the lift-drag ratio. These increases are to be expected, inasmuch as increased toe-in angle adds lifting area to the vehicle lower

surface and increases frontal area. Because the incremental lift produced is behind the vehicle center of gravity, a negative incremental pitching moment is also observed in the comparison of figures 4(a) and 4(b). This increased negative pitching moment will result in lower trim angles of attack for a given δ_e with an increase in toe-in angle, but probably not much loss in trim lift since the lift coefficient increases with toe-in angle.

Detailed data on the configuration with tip fin I_4 and center fin E_2 are presented in figure 5 and are summarized as a trim plot in figure 6. This combination of fins was also tested at supersonic speeds. Results obtained in the Langley Unitary Plan wind tunnel at Mach numbers of 1.5 and 2.16 (not presented herein) show that this combination of fins provided directional stability throughout the test angle-of-attack range and, for this reason, most of the hypersonic data were obtained with these fins. Also presented in figure 6 for comparison are the trim characteristics from reference 3 of the configuration with tip fin D and center fin E. With tip fin I_4, the HL-10 configuration has a maximum L/D of about 1.14 and a maximum C_L of about 0.48, and it is capable of trimming at $L/D = 1$ (at $\alpha = 37^\circ$ and $C_L = 0.35$) for an elevon deflection angle of about 16°. The maximum C_L is about the same and the maximum L/D is slightly higher with tip fin D and center fin E on the configuration. It should also be noted that less positive elevon deflection angles are needed for trim at a given angle of attack with tip fin D, since with the 30° roll-out angle of this fin, more negative pitching moment is produced than with fin I_4, which has an 8.5° roll-out angle.

The incremental pitching moments due to elevon deflection are compared with Newtonian theory in figure 7. For positive elevon deflection angles, the theory greatly overpredicts the experiment at $\alpha = 15^\circ$, but as angle of attack is increased, the overprediction is reduced. An examination of the schlieren flow photographs presented in figure 3 shows that with positive elevon deflections, flow separation occurs ahead of the elevons and would be expected to reduce the elevon effectiveness. The extent of the separation region decreases with increasing angle of attack and thus the results of the comparison of theory and experiment are not totally unexpected. For the theoretical calculation, Newtonian theory ($C_{p,max} = 2$) was used, and no losses due to the blunt-body flow field were considered. Data from reference 3, indicated by squares in figure 7, show that for $\delta_e = 30^\circ$, the incremental pitching moment is greater and thus better agreement between theory and experiment is obtained with tip fin D on the configuration.

In addition to positive elevon deflection angles, two other cases were tested: $\delta_e = -30^\circ$ and elevons off. The data for the elevons off are plotted in figure 7 as flagged symbols at the left borders of the data inserts for $\alpha = 35^\circ$ and $\alpha = 50^\circ$. For the elevons off case, there is very good agreement between the theoretical and experimental incremental pitching moments. For $\delta_e = -30^\circ$ at $\alpha = 50^\circ$, however, the agreement between experimental and theoretical elevon effectiveness is poor. The schlieren flow photographs (fig. 3(e)) for $\alpha \geq 40^\circ$ show the presence of a strong shock wave generated at a longitudinal location approximately coincident with the elevon hinge line.

In order to study this shock and this low effectiveness further, surface flow patterns were obtained by using the oil-flow technique and the results are presented in figure 8. For $\delta_e = 0^\circ$ (fig. 8(a)), the direction of flow over the elevons appears to be parallel to the center line of the vehicle. For $\delta_e = -30^\circ$ (fig. 8(b)), however, the expanded flow over the elevon is turned outward except within the triangular regions adjacent to the elevon tip chords where the oil traces have been wiped off. This lack of oil trace on the tips indicates a region of high shear force. It is possible that vorticity in the region of the elevon tip chords is formed as a result of the difference in pressure across the body-elevon chord plane. This vortex flow could account for the high local pressure in the triangular disturbance regions on the elevons. The high pressure in these regions would certainly contribute to decreasing the elevon effectiveness and thus would account for the differences between theory and experiment.

The shock wave in the vicinity of the expansion over the elevon hinge line is also evident on the configuration with tip fin D for $\delta_e = -60^\circ$. (See fig. 3(f).) For this elevon deflection angle, however, the shock does not form until much higher angles of attack are reached than for $\delta_e = -30^\circ$. For the elevons off case (fig. 3(g)), no strong shock wave is noted in the region of the expansion. Thus it is likely that critical combinations of angle of attack and negative elevon deflection angle are necessary to create the disturbance region on the elevon.

The effects of increasing Reynolds number from 0.7×10^6 to 2.2×10^6 on the longitudinal characteristics of the configuration with $\delta_e = 0^\circ$ are presented in figure 9. Although some effects on axial force and normal force are noted, no effects on the trim angle of attack or stability are noted in the angle-of-attack range of the data. Inasmuch as the schlieren flow photographs show no separated flow for zero elevon deflection, these results may be expected. However, for configurations with positive elevon deflection angles at lower angles of attack, separation is noted to occur ahead of the elevons; therefore, more pronounced Reynolds number effects may be anticipated.

Directional and Lateral Stability Characteristics

Directional and lateral stability measurements were obtained with tip fins I_4, I_5, and I_6. Because of variations in toe-in and roll-out angles among the fins, Newtonian estimates of the stability characteristics for the specific combinations of fin angles tested were made by using the method presented in the appendix. Also included in the appendix are design curves showing the effects of toe-in and roll-out angle on the directional and lateral stability characteristics of a typical tip fin.

In figure 10, Newtonian estimates are presented which show the effects of roll-out angle on the increments in directional and lateral stability (ΔC_{l_β} and ΔC_{n_β}) due to adding tip fins for fins having the same toe-in angles as fins I_4,

I_5, and I_6. The experimental data for these fins are also presented. No definite comparison between theory and experiment can be made with these limited data, but it appears that in most instances the trends are predicted, although the magnitudes are not. These trends are in agreement with the results of a comparison of theory and experiment on another type of vehicle presented in reference 19.

A comparison of the lateral stability characteristics with Newtonian theory for the configuration with tip fins I_4 and with no fins is presented in figure 11. For both configurations, the directional stability parameter C_{n_β} is overestimated, whereas C_{l_β} is underestimated. In general, the trends in the experimental data follow the theoretical results. As was noted in reference 3, elevon deflection is seen to have little effect on the lateral and directional characteristics at hypersonic speeds. The center fin E_2 produces about half the increment in C_{n_β} at $\alpha = 0^\circ$, but its effectiveness diminishes with increasing angle of attack, as would be expected because of shielding effects. (See ref. 3.) Results of reference 3 indicated that the center fin was completely ineffective above $\alpha = 20^\circ$. Inasmuch as the lowest trim angle of attack obtained with I_4 was $\alpha = 16^\circ$ ($\delta_e = 45^\circ$), it is obvious that the center fin has little effect on the hypersonic stability characteristics at trim.

Lateral Control Characteristics

Lateral control characteristics were obtained on the 8-inch (20.32-cm) model for elevon deflection angles of 0°, 15°, and 30°, and aileron deflection angles of 0°, 15°, and 30°. The effects of aileron deflection on the longitudinal characteristics are presented in figure 12, and little effect on C_L, C_D, and L/D is evident. For $\delta_a = 30^\circ$, a negative incremental pitching moment is obtained; it is caused by the higher loading on the elevon deflected into the wind as compared with the loading on the elevon deflected away from the wind. For $\delta_e = 30^\circ$, this negative incremental pitching moment results in about a 2° lower trim angle of attack. The basic lateral control characteristics are presented throughout the test angle-of-attack range in figure 13 and are summarized in figure 14 for several angles of attack. One important trend to be noted in figure 14 is the strong dependence of lateral control on elevon deflection angle. For example, at $\alpha = 25^\circ$, the ailerons are about four times as effective for $\delta_e = 30^\circ$ as they are for $\delta_e = 0^\circ$. The increase in control effectiveness with increasing angle of attack and increasing elevon deflection angle is a result of the high-pressure coefficients on the elevons at the high flow deflection angles. Also, because of the canted elevon hinge line, the yawing moment due to roll control is very small. No comparison of roll control effectiveness with Newtonian theory has been made since the elevon effectiveness (which is indicative of roll control, since the elevons are used for roll control also) shows poor agreement with theory in figure 7.

CONCLUDING REMARKS

The effects of modifications of the tip fins and center fin on the aerodynamic characteristics of a model of a manned lifting entry vehicle with negative camber, a flat bottom, a blunt leading edge, and a delta planform (designated HL-10) have been determined at a Mach number of 6.8. The configuration with modified tip and center fins was directionally and laterally stable throughout the test angle-of-attack range. The maximum trimmed lift coefficient obtained was 0.48 and the maximum trimmed lift-drag ratio was about 1.14. Roll-control effectiveness increased with increasing angle of attack and with increasing positive elevon deflection angle. The yawing moment due to roll control was very small.

Newtonian theory generally predicts the trends in incremental, directional, and lateral stability of tip fins due to fin toe-in and roll-out angles, but does not give close estimates of the magnitudes. Simple Newtonian theory does not predict the incremental pitching moment due to elevon deflection because of the complex flow field over the elevons at both positive and negative deflection angles.

Langley Research Center,
National Aeronautics and Space Administration,
Langley Station, Hampton, Va., August 4, 1965.

APPENDIX

COMPUTATION OF INCREMENTAL DIRECTIONAL AND LATERAL STABILITY OF TIP FINS

Equations to determine the directional and lateral stability characteristics of tip fins on hypersonic lifting vehicles have been derived by using Newtonian flow concepts. The effects of fin toe-in and roll-out angle were included in the calculations, which are for the windward fin surface. The effects of fin leading edge on directional and lateral stability were found to be small and are not included in the calculations. Results obtained from these equations, showing the effects of fin roll-out angle on C_{n_β}, have been presented in reference 20 for a fin toe-in angle of 10° at angles of attack from 0° to 60°. Experimental results for various fin roll-out angles were also obtained at $M = 6.8$, and the parameters C_{l_β}, C_{n_β}, and C_{Y_β} are compared with the Newtonian calculations in reference 19.

These equations have been also used to compute the influence of the fins on directional and lateral stability for the model of the HL-10 presented in the present paper. Although the derivation of these equations is not difficult, it is very time consuming, and, for this reason, only the equations are presented herein as follows:

$$C_{l_\beta} = -K(\cos\alpha \sin\epsilon \cos\phi' - \sin\alpha \sin\phi')\left(\frac{z_F}{b}\cos\epsilon\cos\phi' - \frac{y_F}{b}\sin\phi\right) \quad (1)$$

$$C_{n_\beta} = K(\cos\alpha \sin\epsilon \cos\phi' - \sin\alpha \sin\phi')\left(\frac{x_F}{b}\cos\epsilon\cos\phi + \frac{y_F}{b}\sin\epsilon\cos\phi'\right) \quad (2)$$

$$C_{Y_\beta} = -K(\cos\alpha \sin\epsilon \cos\phi' - \sin\alpha \sin\phi')(\cos\epsilon\cos\phi') \quad (3)$$

where $K = \frac{4}{57.3} C_{p,max} \frac{S_F}{S} \cos 2\beta \cos\epsilon \cos\phi'$. For small values of ϵ and ϕ ($\cos\epsilon = \cos\phi' = 1$; $\sin\epsilon = \epsilon$, $\sin\phi' = \phi'$), these equations are identical to the equations derived and presented in reference 21.

In order to show the effects of fin toe-in and roll-out angle on the incremental lateral stability, plots of equations (1), (2), and (3) are presented in figure 15. For this figure, the following constants were used:

$$\frac{S_F}{S} = 0.10$$

$$\frac{x_F}{b} = 0.50$$

$$\frac{y_F}{b} = 0.50$$

$$\frac{z_F}{b} = 0.10$$

$$C_{p,max} = 2.0$$

The curves in figure 15 may be used for any configuration if the differences in fin area and transfer distance are accounted for in the use of the equations presented.

REFERENCES

1. Rainey, Robert W.; and Ladson, Charles L.: Preliminary Aerodynamic Characteristics of a Manned Lifting Entry Vehicle at a Mach Number of 6.8. NASA TM X-844, 1963.

2. Ware, George M.: Aerodynamic Characteristics of Models of Two Thick 74° Delta Manned Lifting Entry Vehicles at Low-Subsonic Speeds. NASA TM X-914, 1964.

3. Ladson, Charles L.: Aerodynamic Characteristics of a Manned Lifting Entry Vehicle at a Mach Number of 6.8. NASA TM X-915, 1964.

4. Dunavant, James C.; and Everhart, Philip E.: Investigation of the Heat Transfer to the HL-10 Manned Lifting Entry Vehicle at a Mach Number of 8. NASA TM X-998, 1964.

5. Rainey, Robert W.; and Ladson, Charles L.: Aerodynamic Characteristics of a Manned Lifting Entry Vehicle at Mach Numbers From 0.2 to 1.2. NASA TM X-1015, 1964.

6. McShera, John T., Jr.; and Campbell, James F.: Stability and Control Characteristics of a Manned Lifting Entry Vehicle at Mach Numbers From 2.29 to 4.63. NASA TM X-1019, 1964.

7. Campbell, James F.; and McShera, John T., Jr.: Stability and Control Characteristics From Mach Number 1.50 to 2.86 of a Model of a Manned Lifting Entry Vehicle. NASA TM X-1117, 1965.

8. McShera, John T., Jr.; and Campbell, James F.: Aerodynamic Characteristics From Mach 1.50 to 2.86 of a Lifting Entry Vehicle Alone, With Adapter Sections, and With a Saturn Launch Vehicle. NASA TM X-1125, 1965.

9. Silvers, H. Norman; and Campbell, James F.: Stability Characteristics of a Manned Lifting Entry Vehicle With Various Fins at Mach Numbers From 1.50 to 2.86. NASA TM X-1161, 1965.

10. Johnston, Patrick J.: Stability Characteristics of a Manned Lifting Entry Vehicle at a Mach Number of 20.3 in Helium. NASA TM X-1156, 1965.

11. Harvey, William D.: Pressure Distribution on HL-10 Manned Lifting Entry Vehicle at a Mach Number of 19.5. NASA TM X-1135, 1965.

12. Harris, Julius E.: Longitudinal Aerodynamic Characteristics of a Manned Lifting Entry Vehicle at a Mach Number of 19.7. NASA TM X-1080, 1965.

13. Everhart, Philip E.; and Hamilton, H. Harris: Investigation of Roughness-Induced Turbulent Heating to the HL-10 Manned Lifting Entry Vehicle at a Mach Number of 8. NASA TM X-1101, 1965.

14. Ware, George M.: Effect of Fin Arrangements on Aerodynamic Characteristics of a Thick 74° Delta Manned Lifting Entry Vehicle at Low-Subsonic Speeds. NASA TM X-1020, 1965.

15. Spencer, Bernard, Jr.: An Investigation of Methods of Improving Subsonic Performance of a Manned Lifting Entry Vehicle. NASA TM X-1157, 1965.

16. Rainey, Robert W.: Summary of an Advanced Manned Lifting Entry Vehicle Study. NASA TM X-1159, 1965.

17. Mechtly, E. A.: The International System of Units - Physical Constants and Conversion Factors. NASA SP-7012, 1964.

18. Bertram, Mitchel H.: Exploratory Investigation of Boundary-Layer Transition on a Hollow Cylinder at a Mach Number of 6.9. NACA Rept. 1313, 1957. (Supersedes NACA TN 3546.)

19. Ladson, Charles L.: Directional and Lateral Stability Characteristics of a Winged Reentry Vehicle at Hypersonic Speeds. NASA TM X-550, 1961.

20. Rainey, Robert W.; and Close, William H.: Studies of Stability and Control of Winged Reentry Configurations. NASA TM X-327, 1960.

21. Hankey, Wilbur L., Jr.; and Alexander, Grover L.: Prediction of Hypersonic Aerodynamic Characteristics for Lifting Vehicles. ASD-TDR-63-668, U.S. Air Force, 1963.

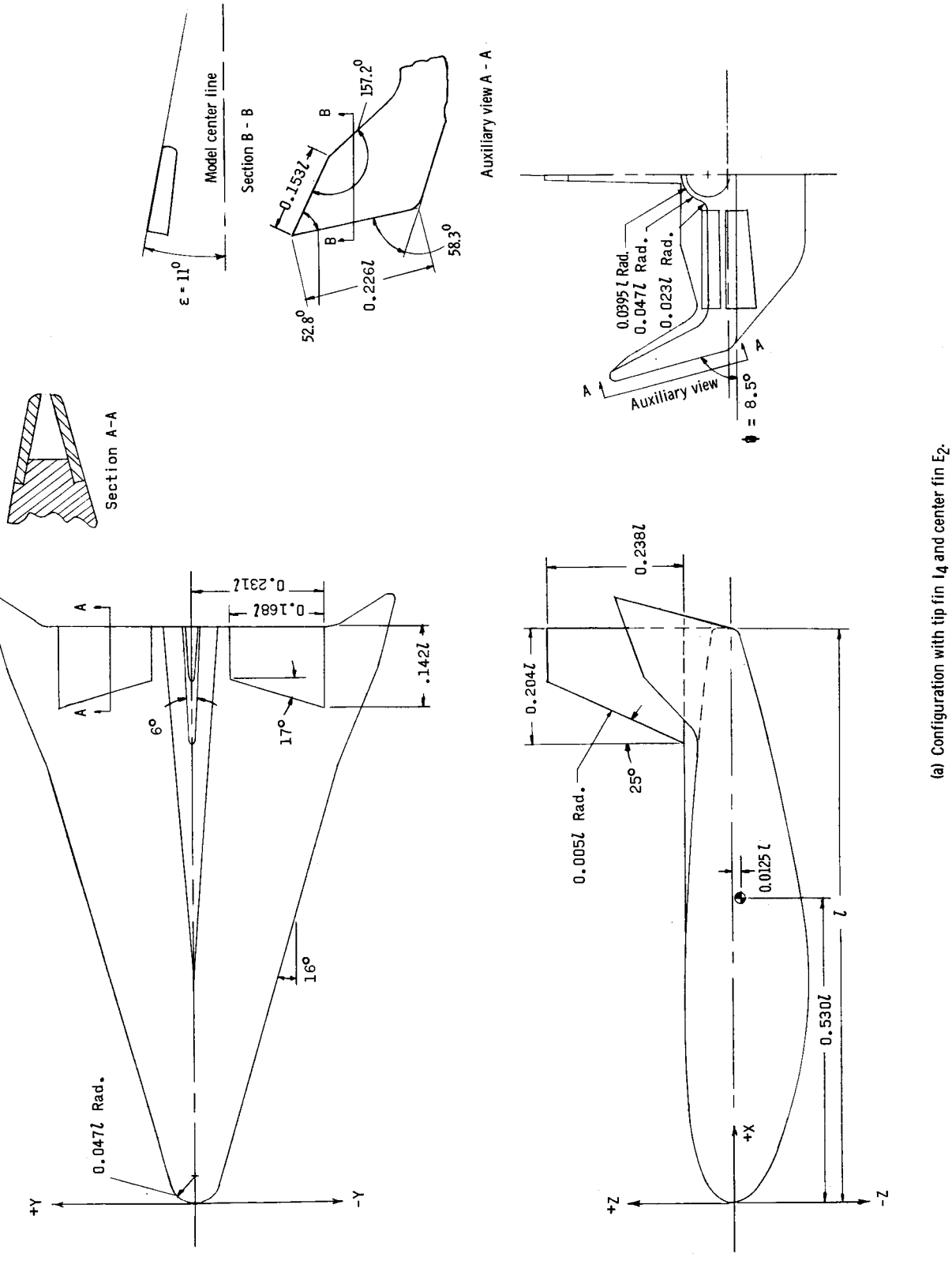

(a) Configuration with tip fin l_4 and center fin E_2.

Figure 1.- Model drawings and dimensions.

(b) Cross sections.

Figure 1.- Continued.

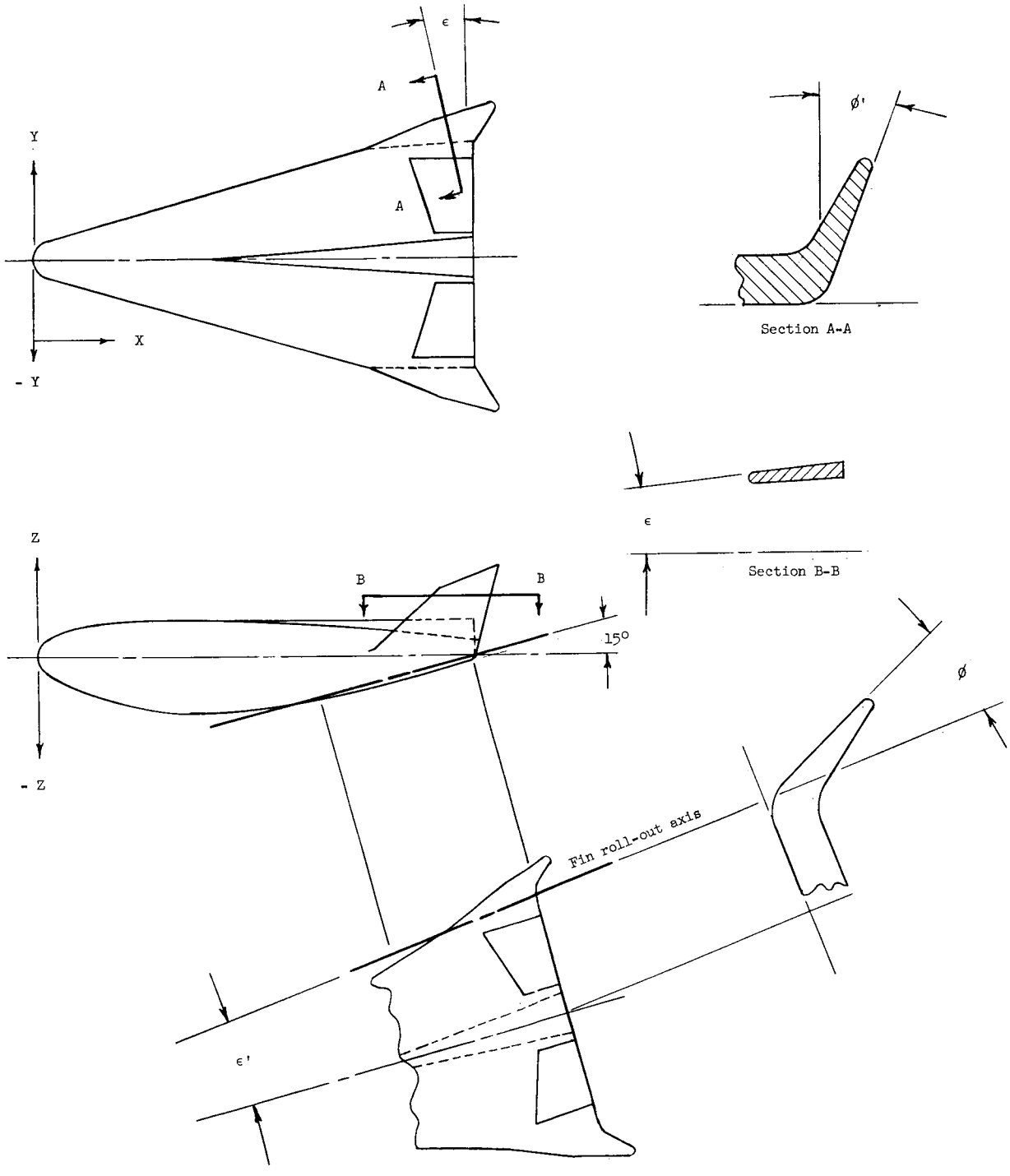

(c) Fin toe-in and roll-out angle definitions.

Figure 1.- Concluded.

L-65-3797

(a) Tip fin I_4, center fin E_2 and $\delta_e = 0^o$.

Figure 2.- Photographs of 8-inch (20.32-cm) model.

L-63-8151

(b) Tip fin D, center fin E, and $\delta_e = 0^0$. (From ref. 3.)

Figure 2.- Concluded.

L-65-171

(a) $\delta_e = 45^0$.

Figure 3.- Schlieren flow photographs.

L-65-172

(b) $\delta_e = 30^0$.

Figure 3.- Continued.

L-65-173

(c) $\delta_e = 15^o$.

Figure 3.- Continued.

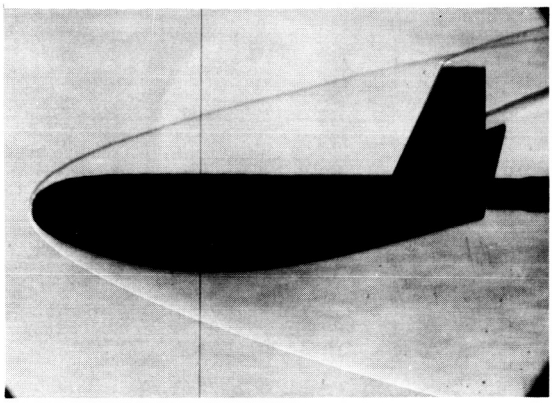

α = 0°

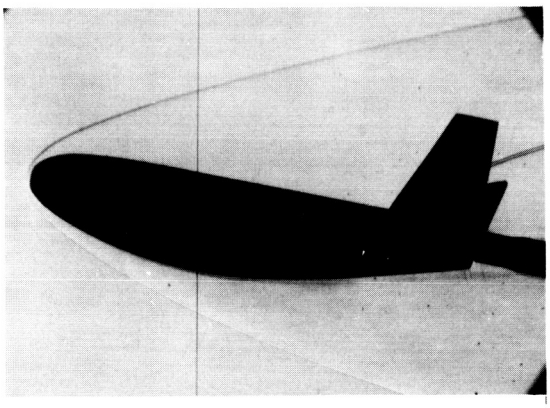

α = 10°

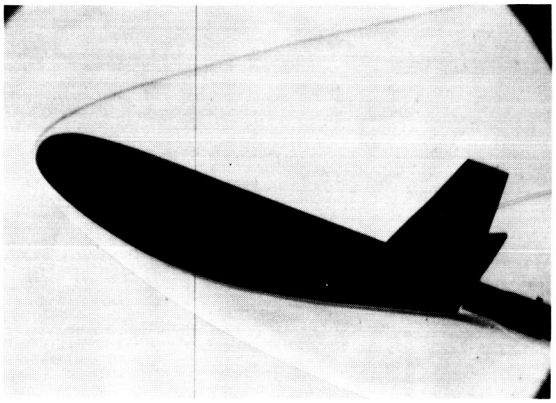

α = 20°

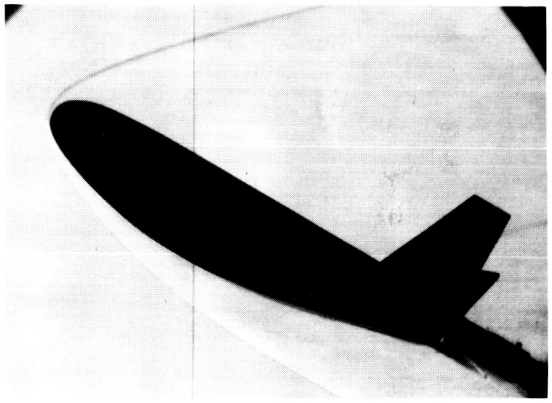

α = 30°

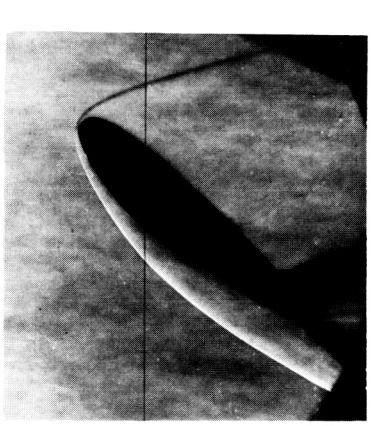

α = 40°

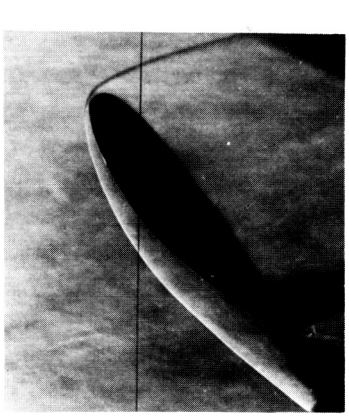

α = 50°

(d) $\delta_e = 0^0$.

L-65-174

Figure 3.- Continued.

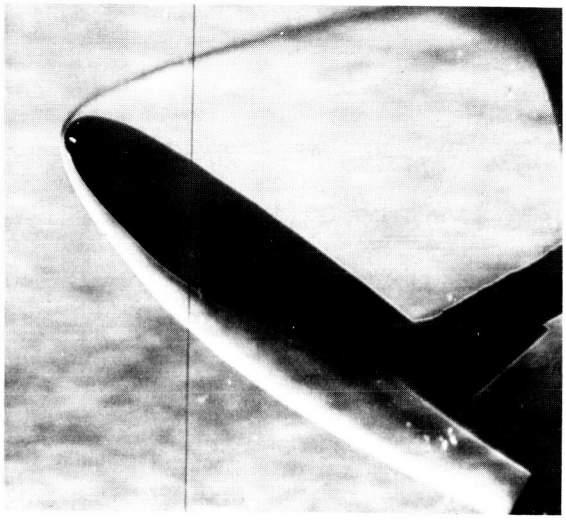

α = 32°

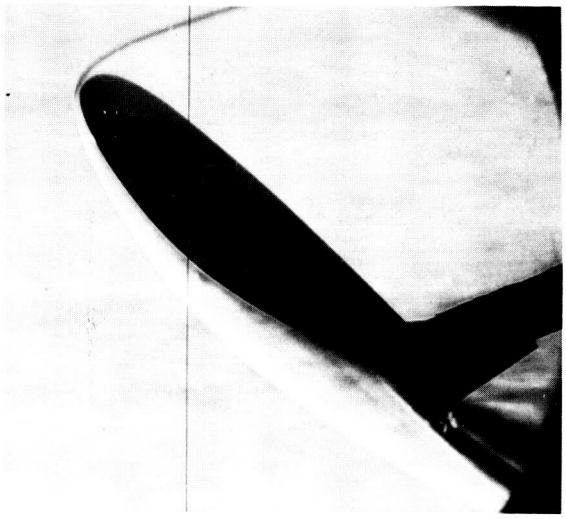

α = 40°

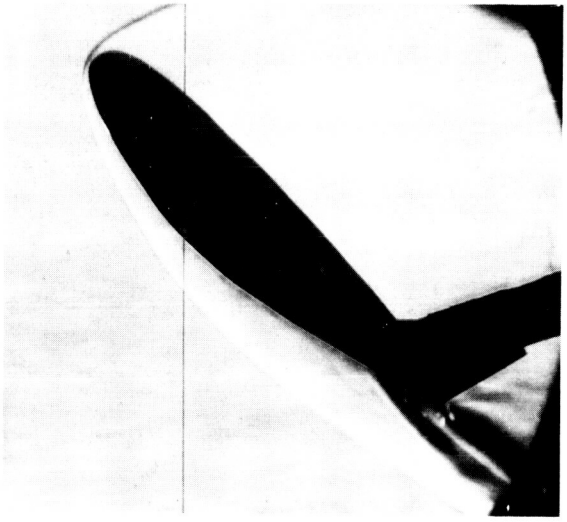

α = 44°

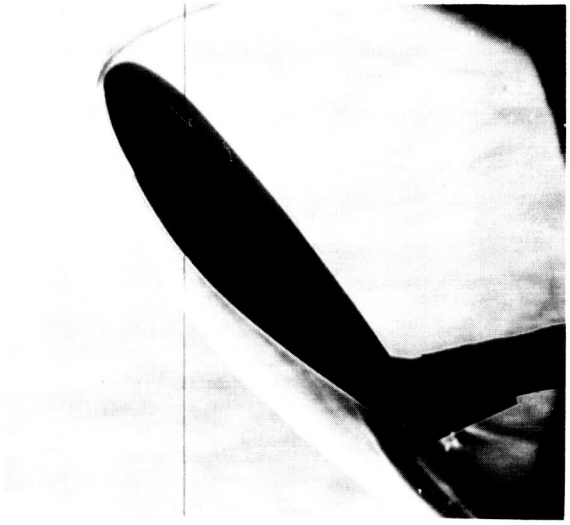

α = 50°

(e) $\delta_e = -30^o$.

L-65-175

Figure 3.- Continued.

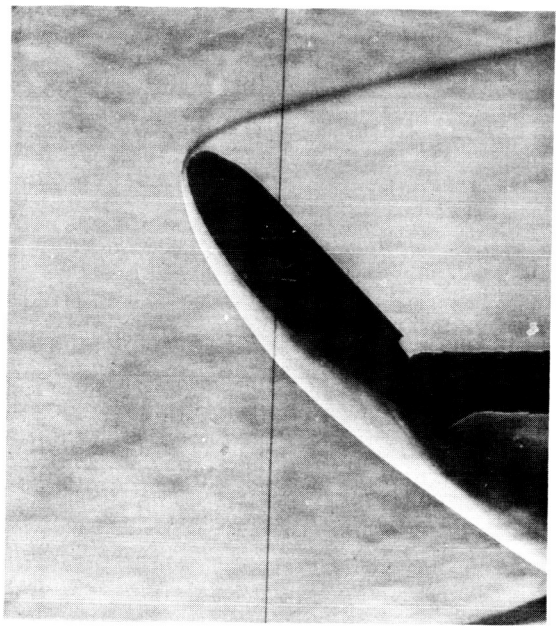

α = 45°

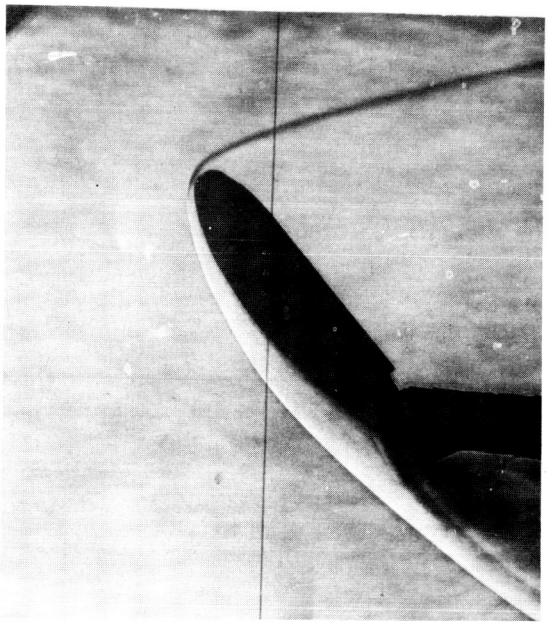

α = 50°

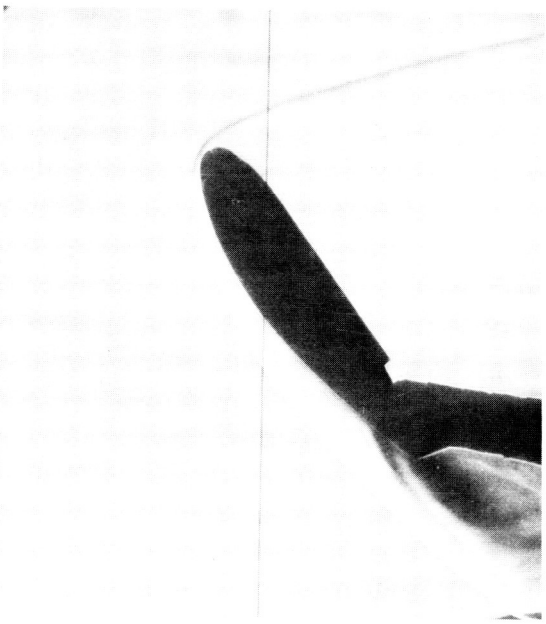

α = 55°

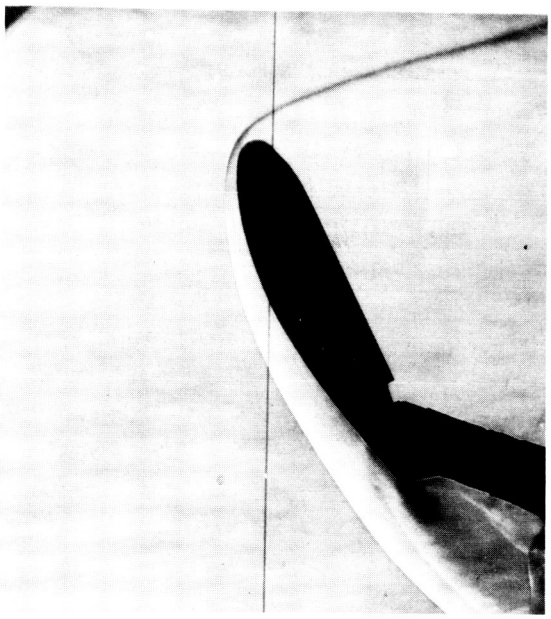

α = 65°

(f) $\delta_e = -60^0$.

L-65-176

Figure 3.- Continued.

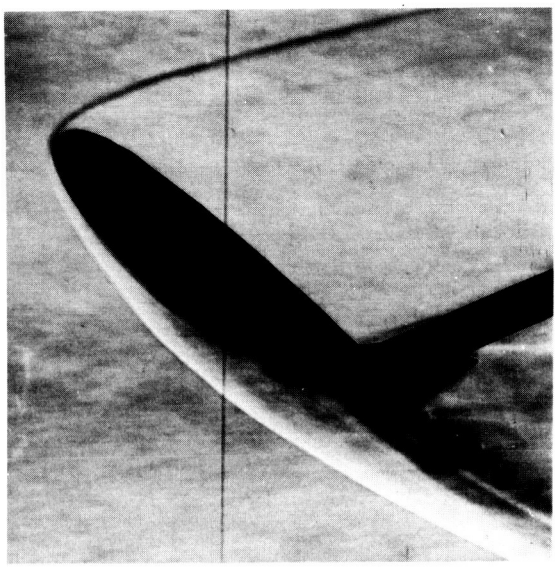

α = 36°

α = 40°

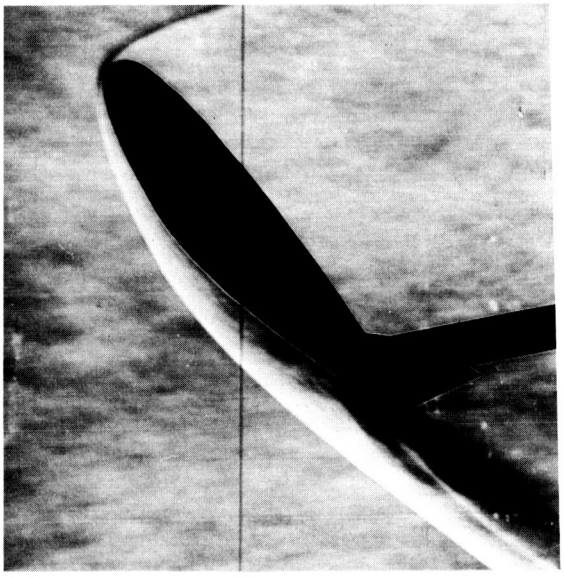

α = 48°

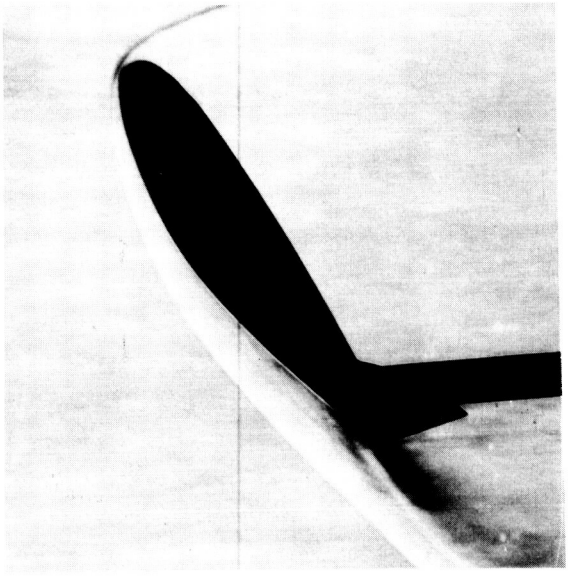

α = 54°

(g) Elevons off.

L-65-177

Figure 3.- Concluded.

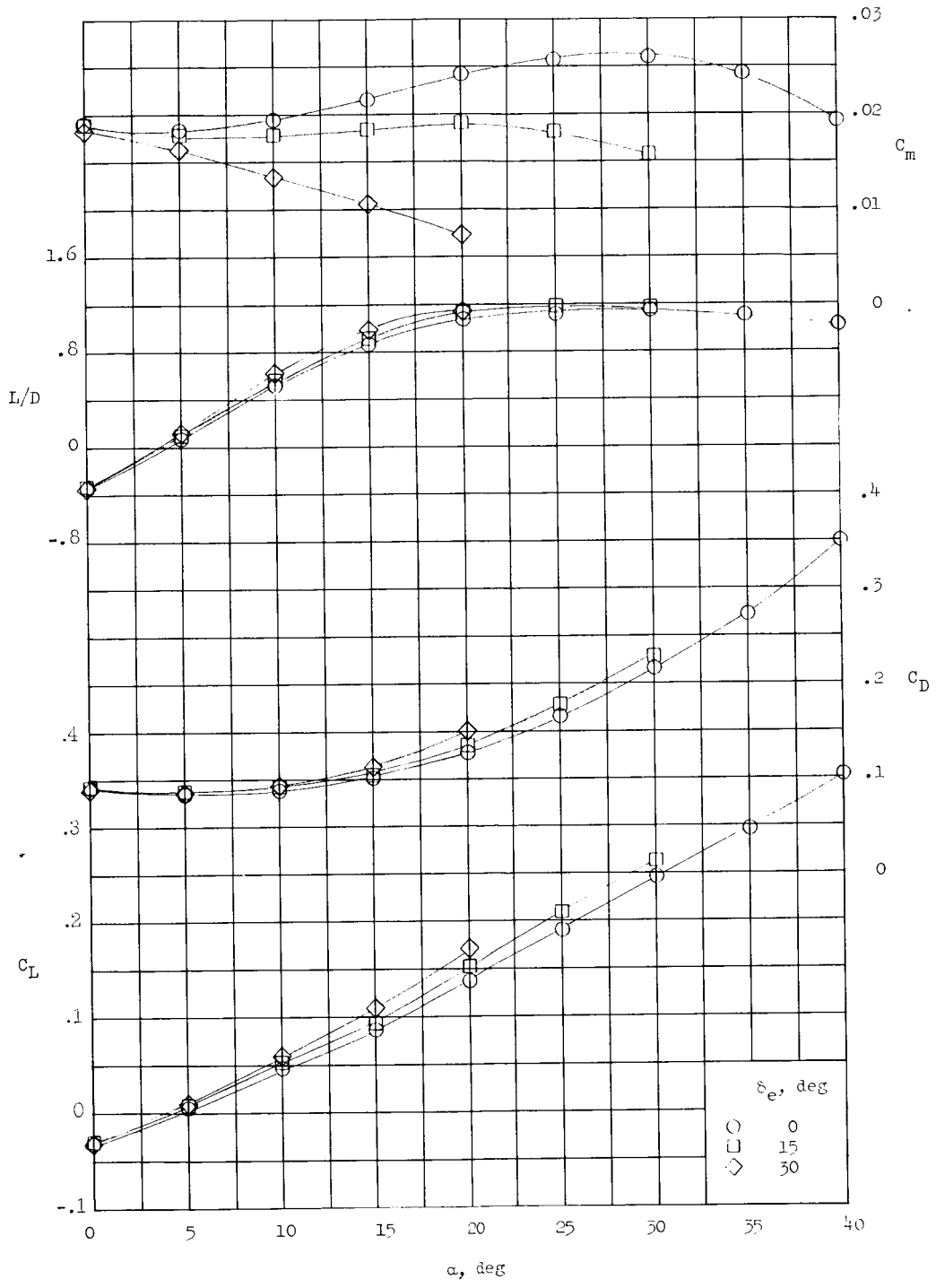

(a) Tip fin I_5 and center fin E_2.

Figure 4.- Effects of tip-fin toe-in angle on longitudinal performance and control.

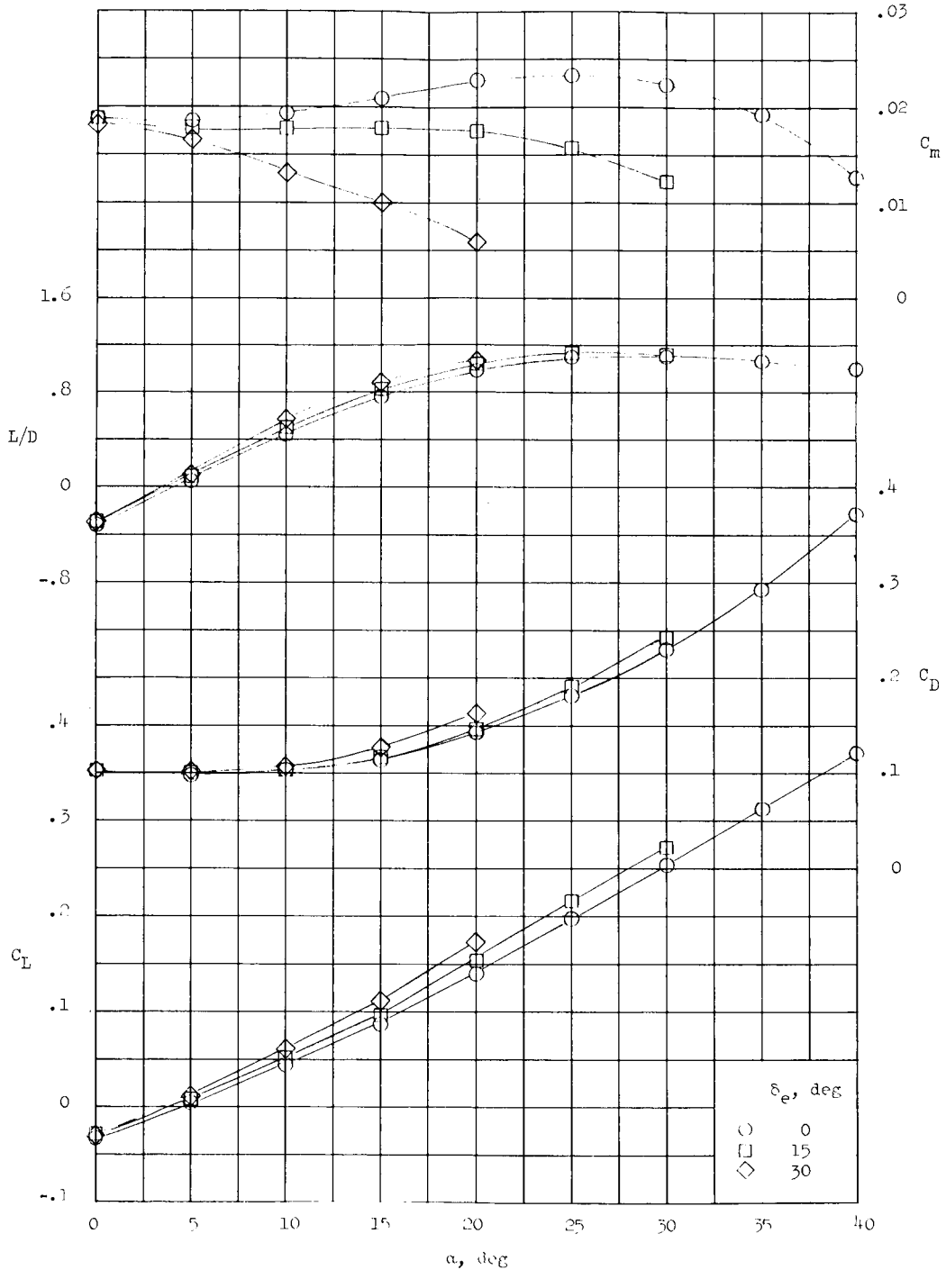

(b) Tip fin I_6 and center fin E_2.

Figure 4.- Concluded.

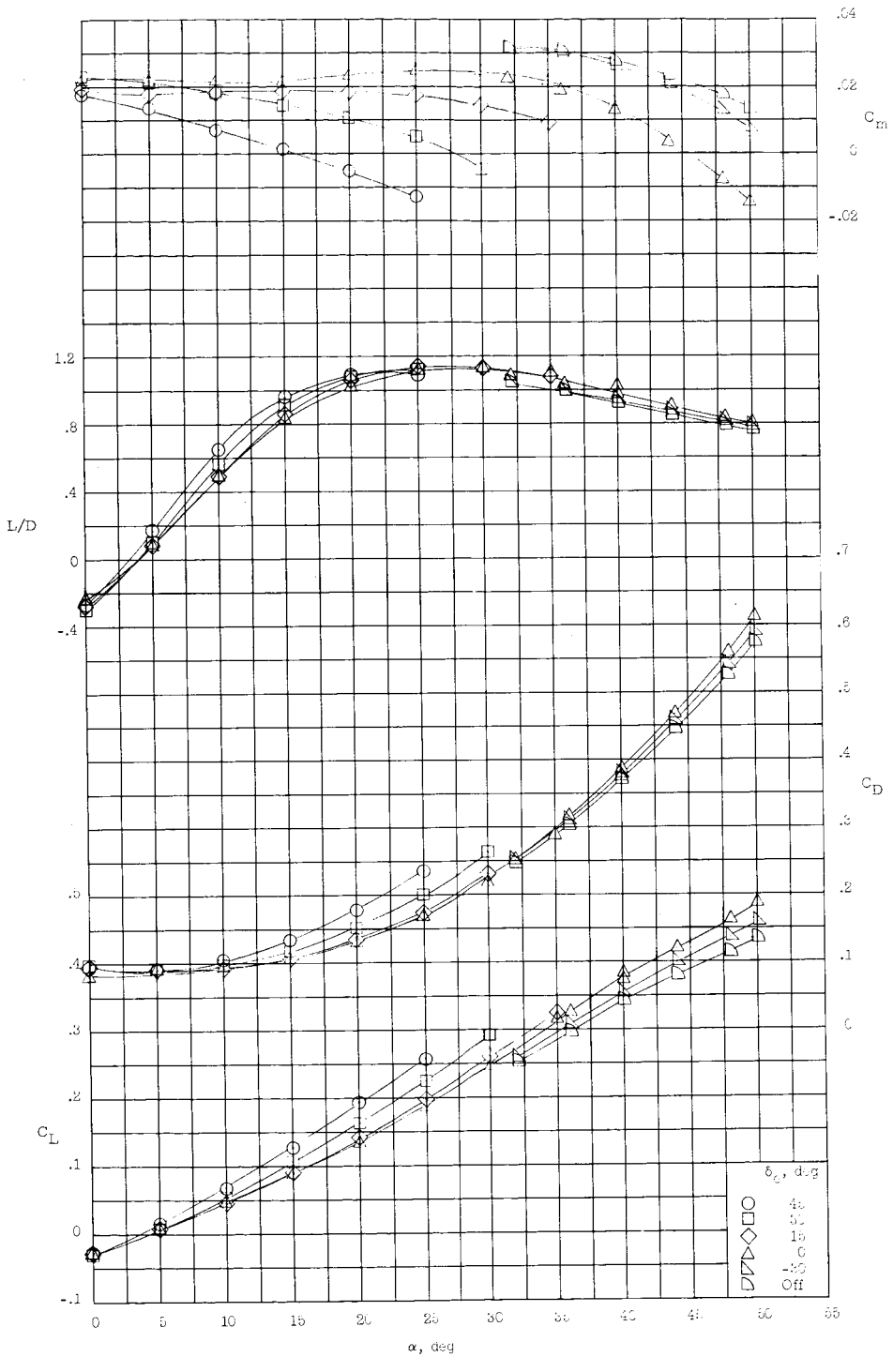

(a) Longitudinal performance.

Figure 5.- Effects of elevon deflection on longitudinal characteristics of configuration with tip fin I_4 and center fin E_2.

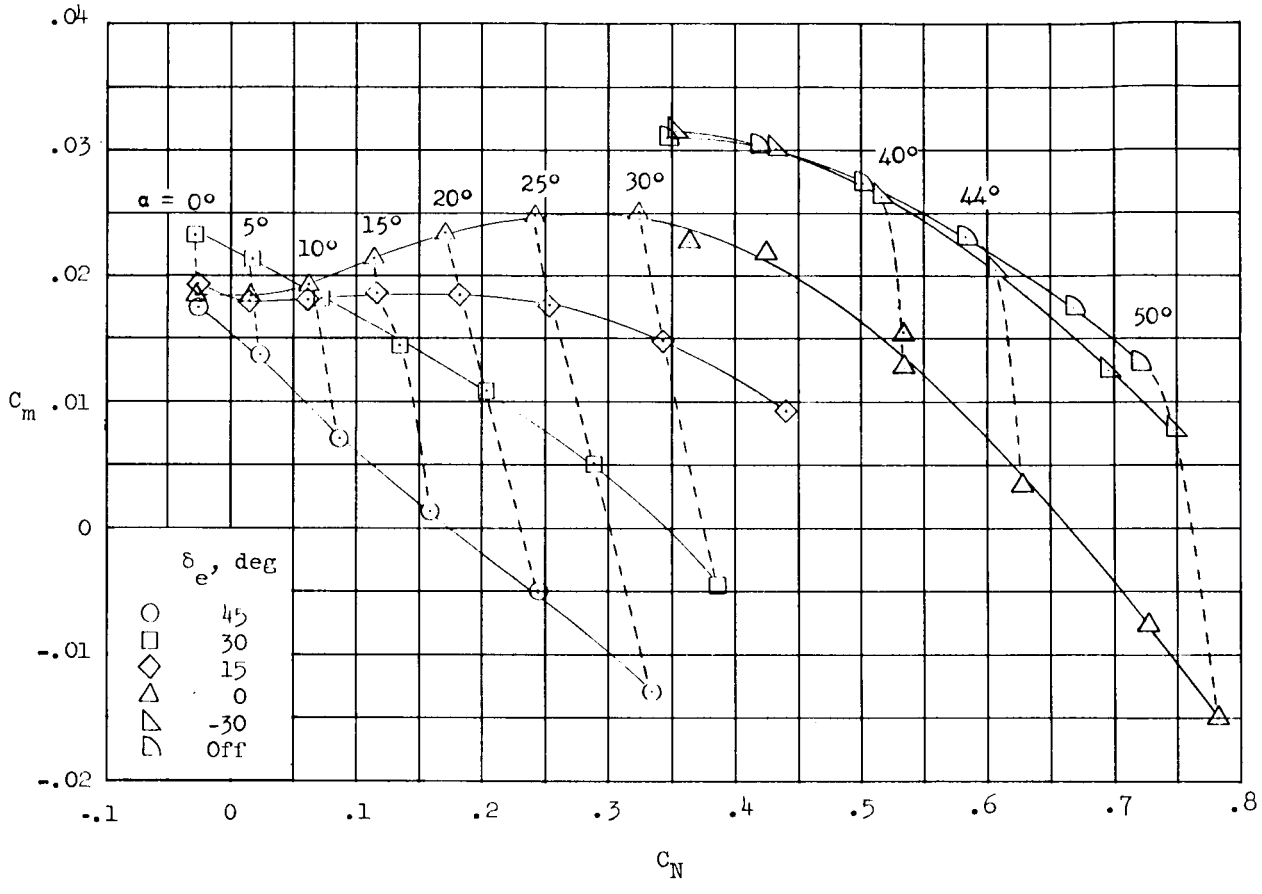

(b) Longitudinal control.

Figure 5.- Concluded.

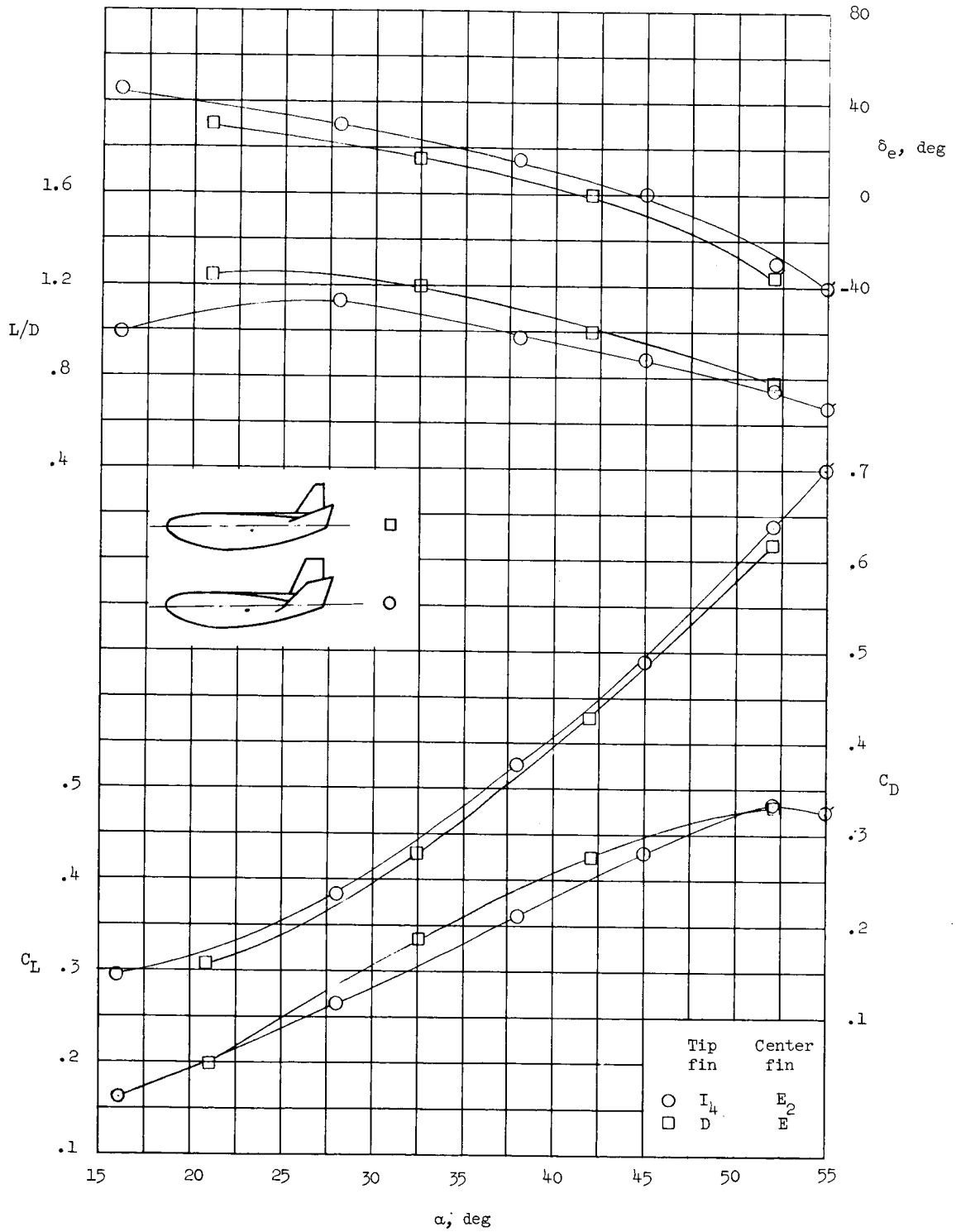

Figure 6.- Comparison of trim characteristics of configuration with tip fin I_4 and center fin E_2; and tip fin D and center fin E. (D and E fin data from ref. 3.)

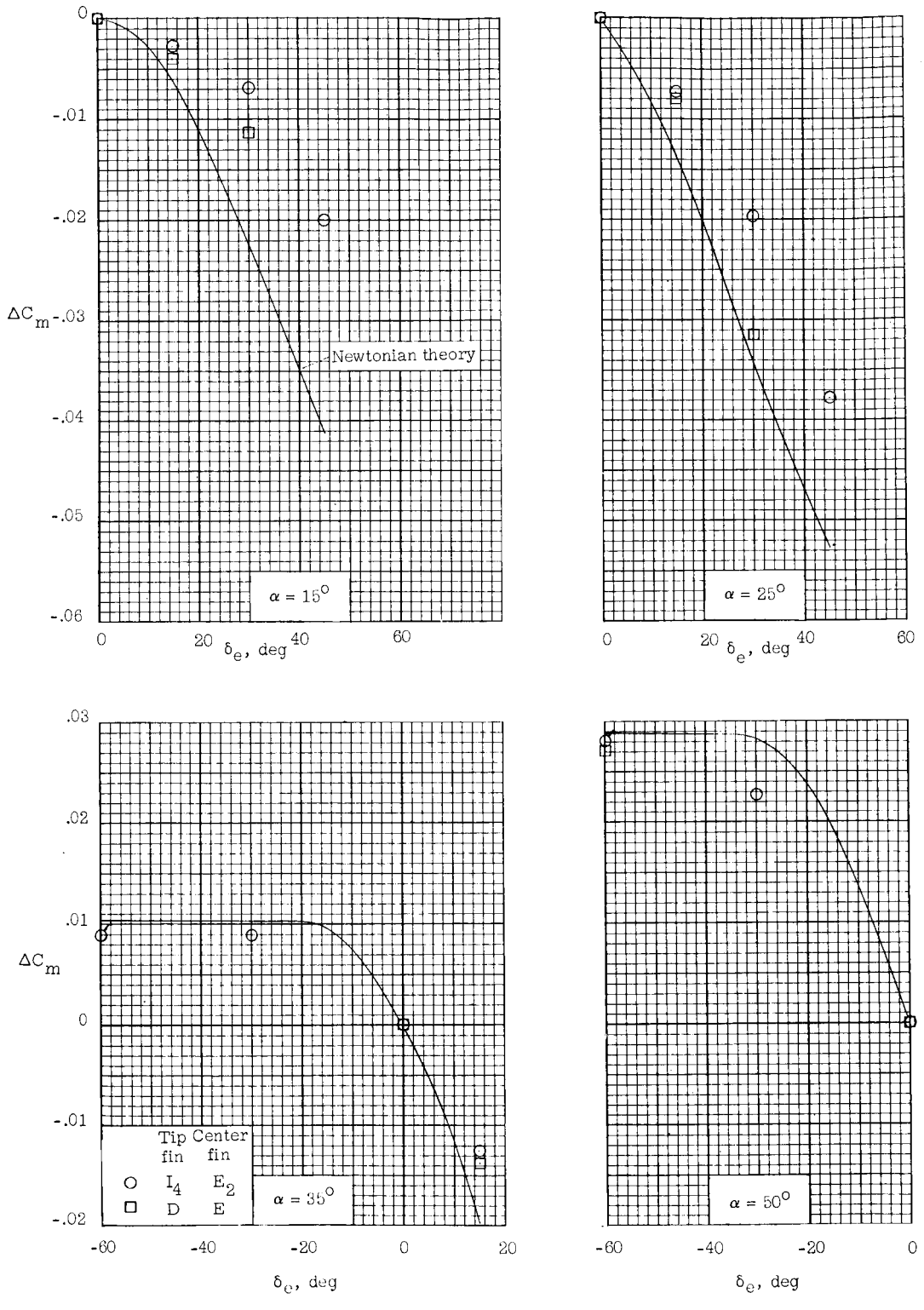

Figure 7.- Comparison of elevon effectiveness with Newtonian theory. (Flagged symbols indicate elevon off.)

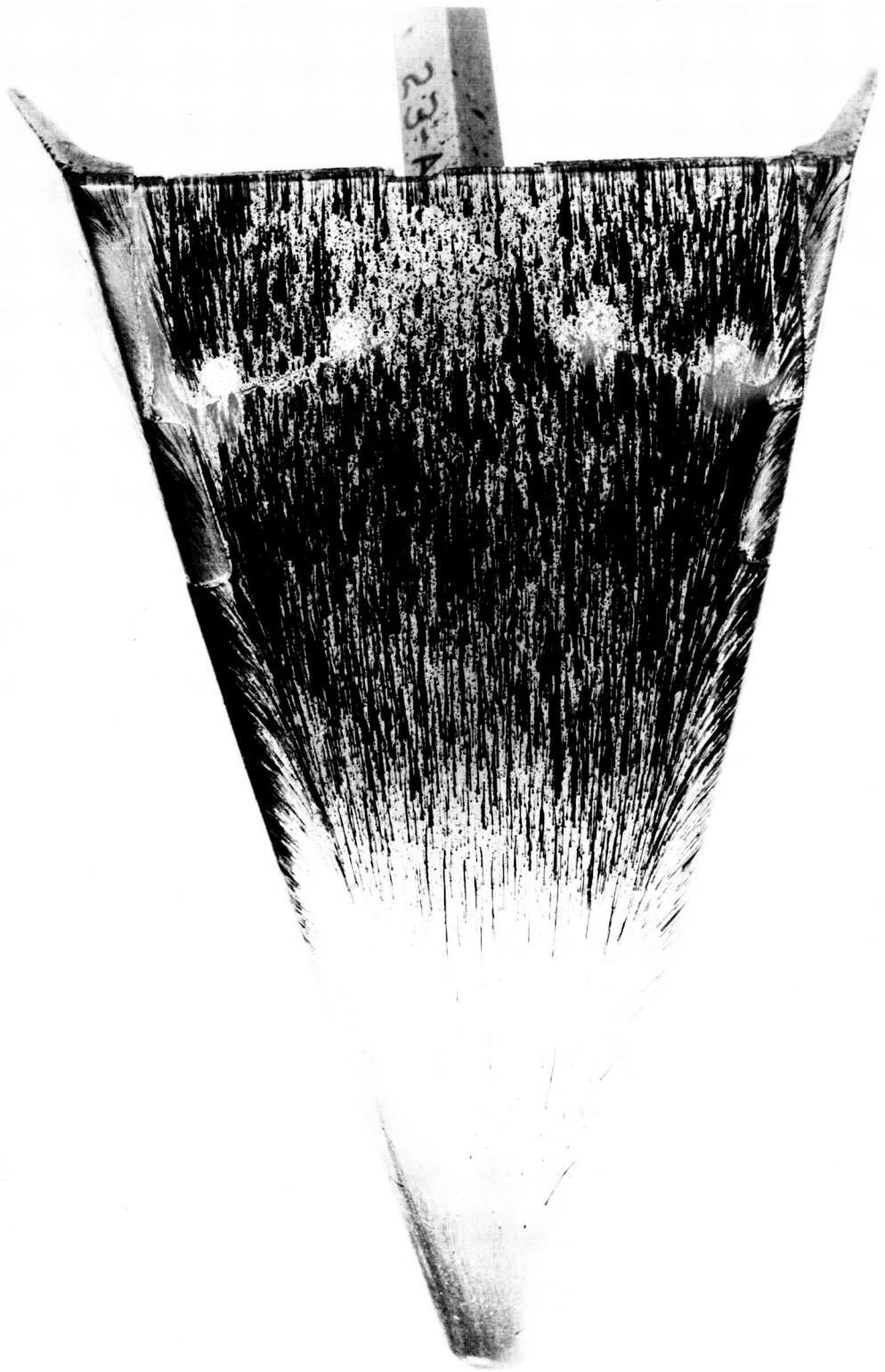

L-65-3327

(a) $\delta_e = 0^o$.

Figure 8.- Lower surface oil-flow pattern. $\alpha = 44^o$.

L-65-3325

(b) $\delta_e = -30^0$.

Figure 8.- Concluded.

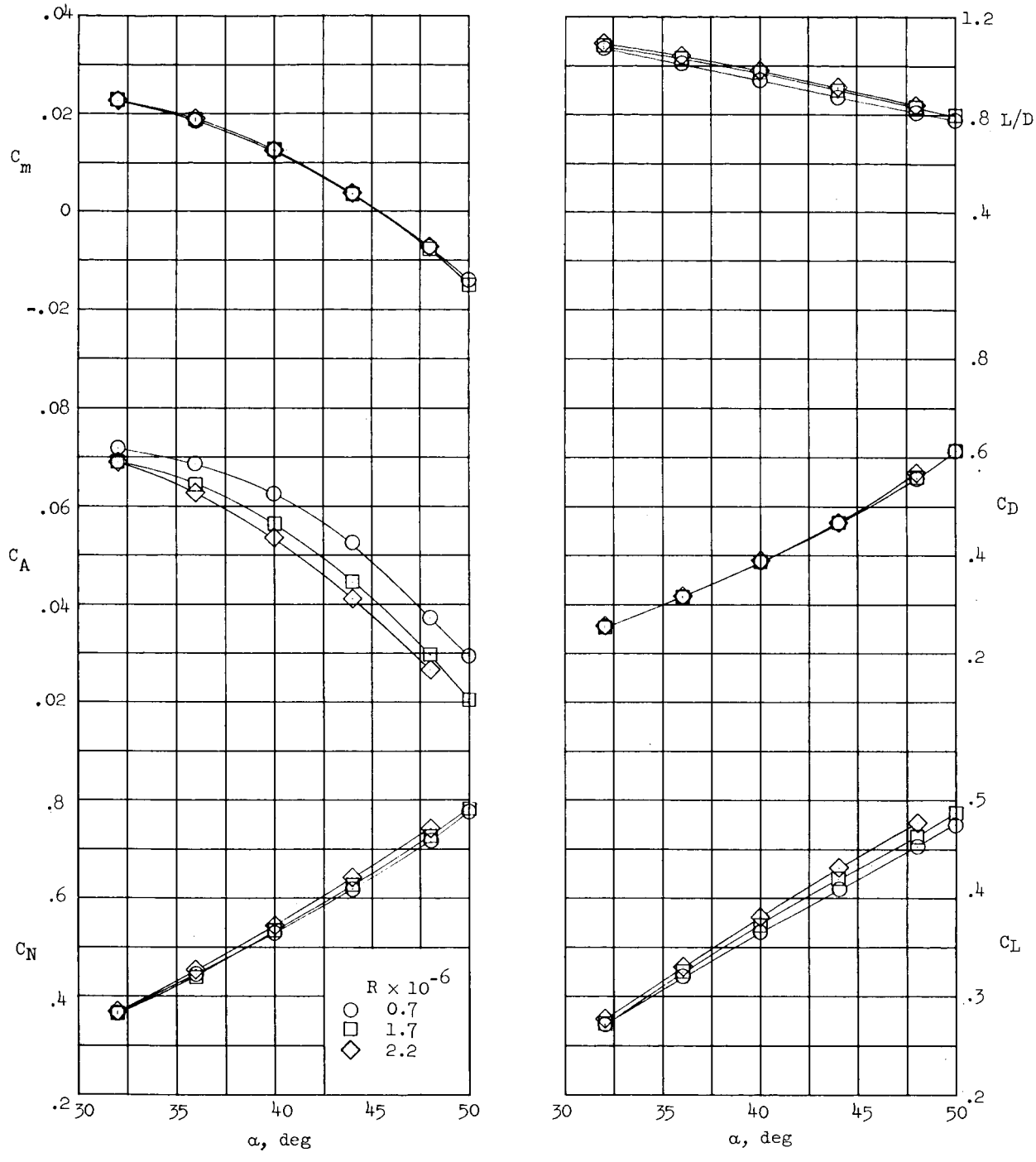

Figure 9.- Effects of Reynolds number on longitudinal characteristics of configuration with tip fin I_4 and center fin E_2. $\delta_e = 0^0$.

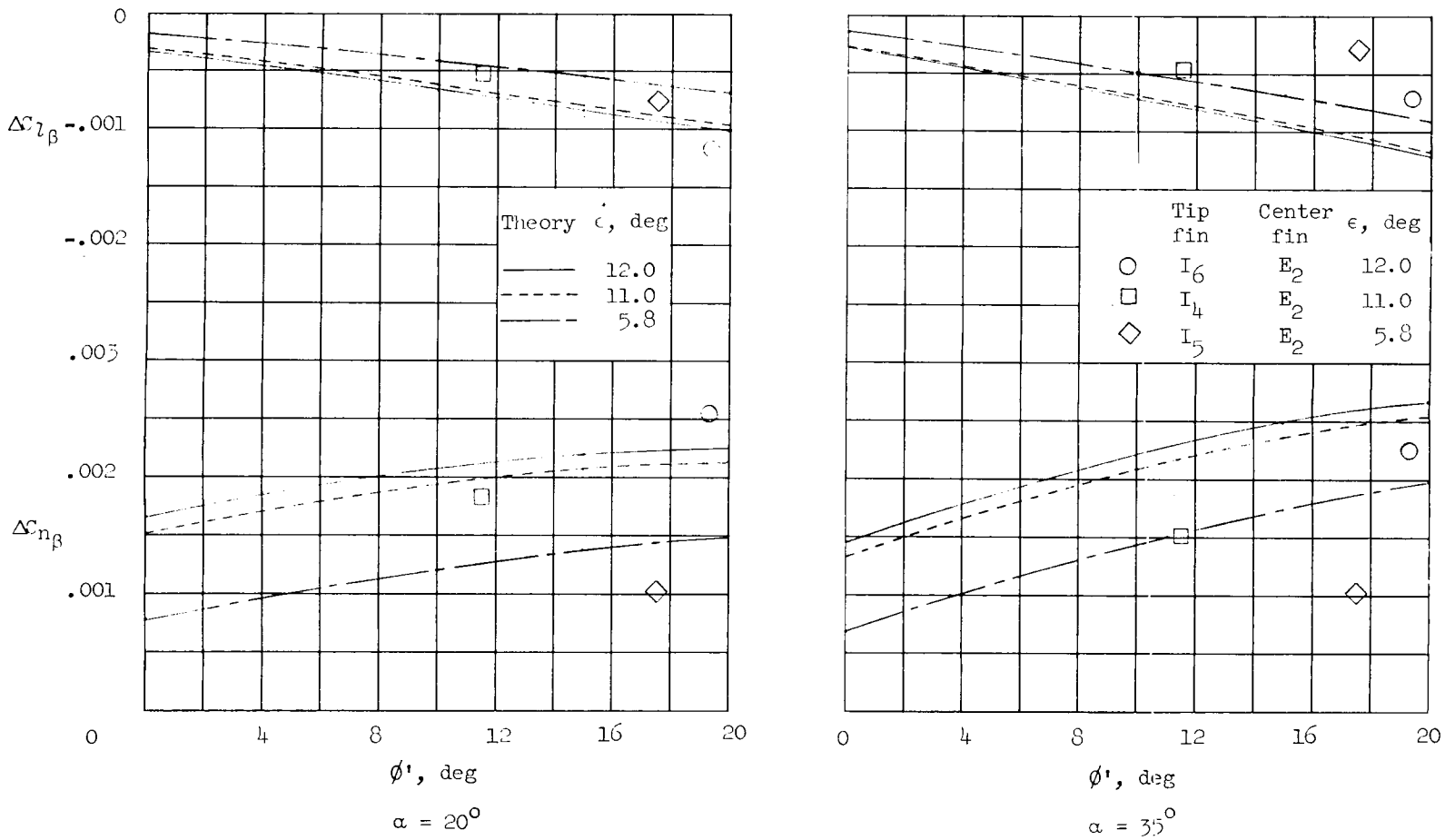

Figure 10.- Comparison of incremental, directional, and lateral stability parameters with Newtonian theory.

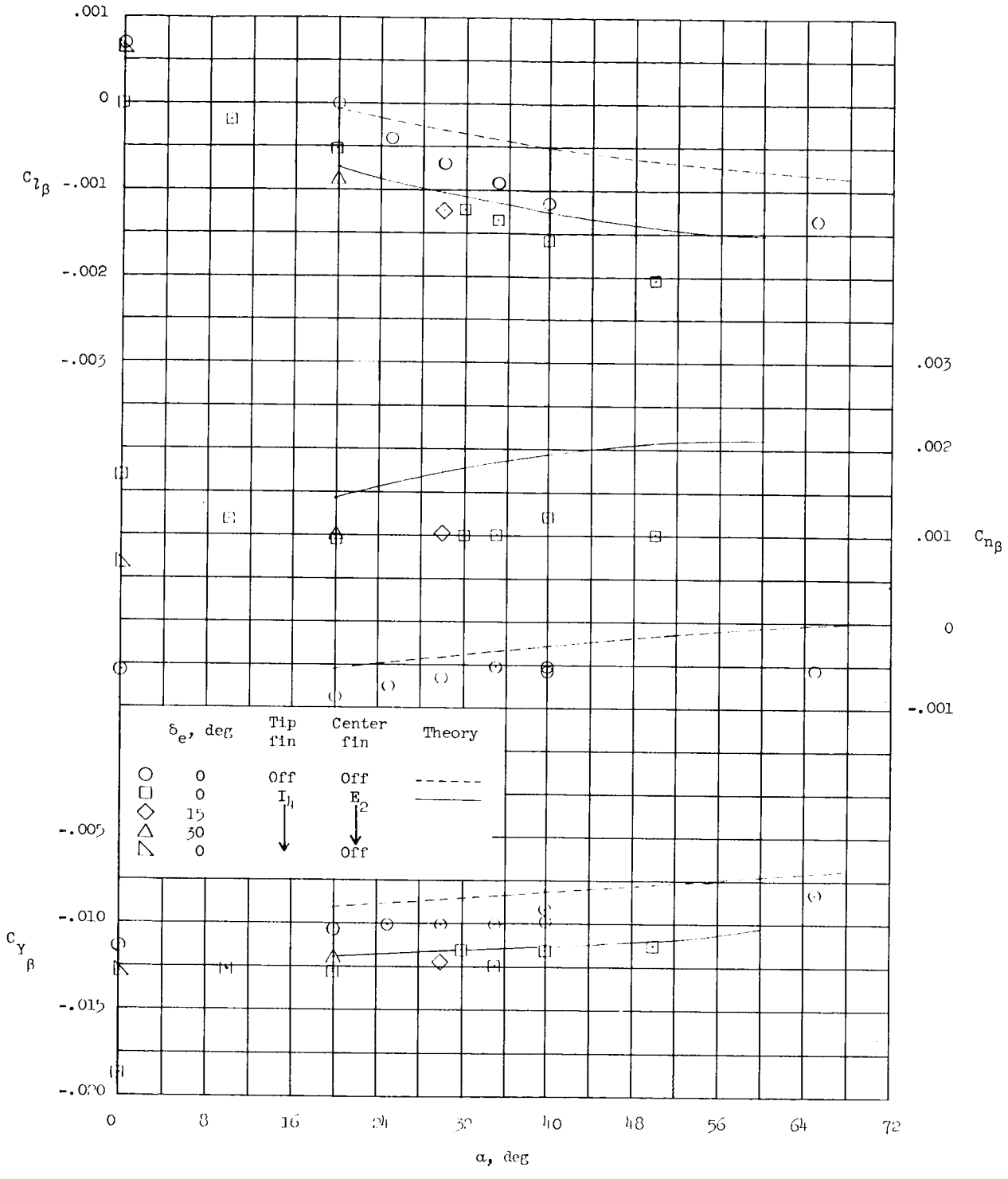

Figure 11.- Comparison of experimental lateral stability parameters with Newtonian theory for configuration with tip fin I_4 and no tip fins.

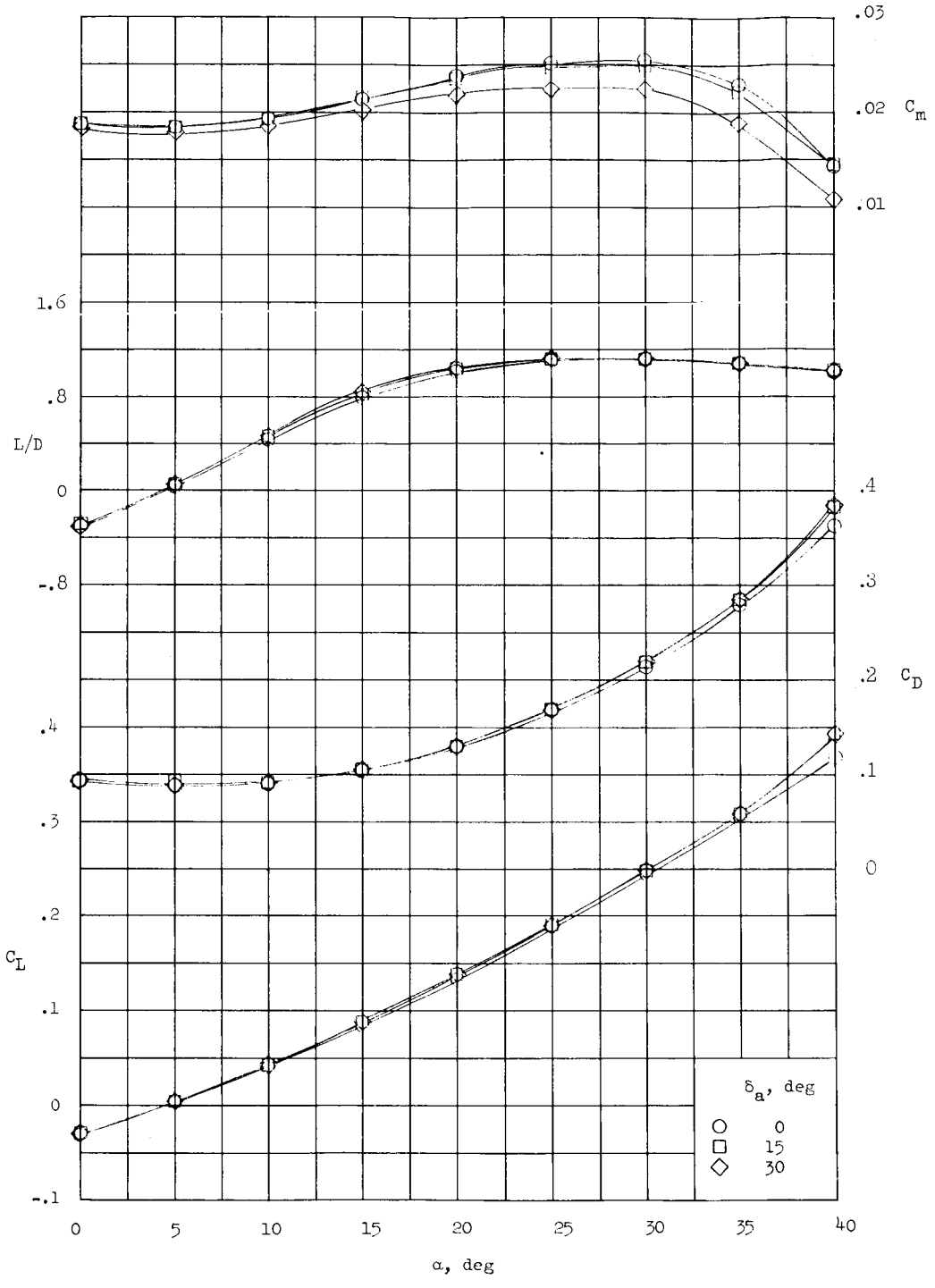

(a) $\delta_e = 0^0$.

Figure 12.- Effects of aileron deflection on longitudinal aerodynamic characteristics.

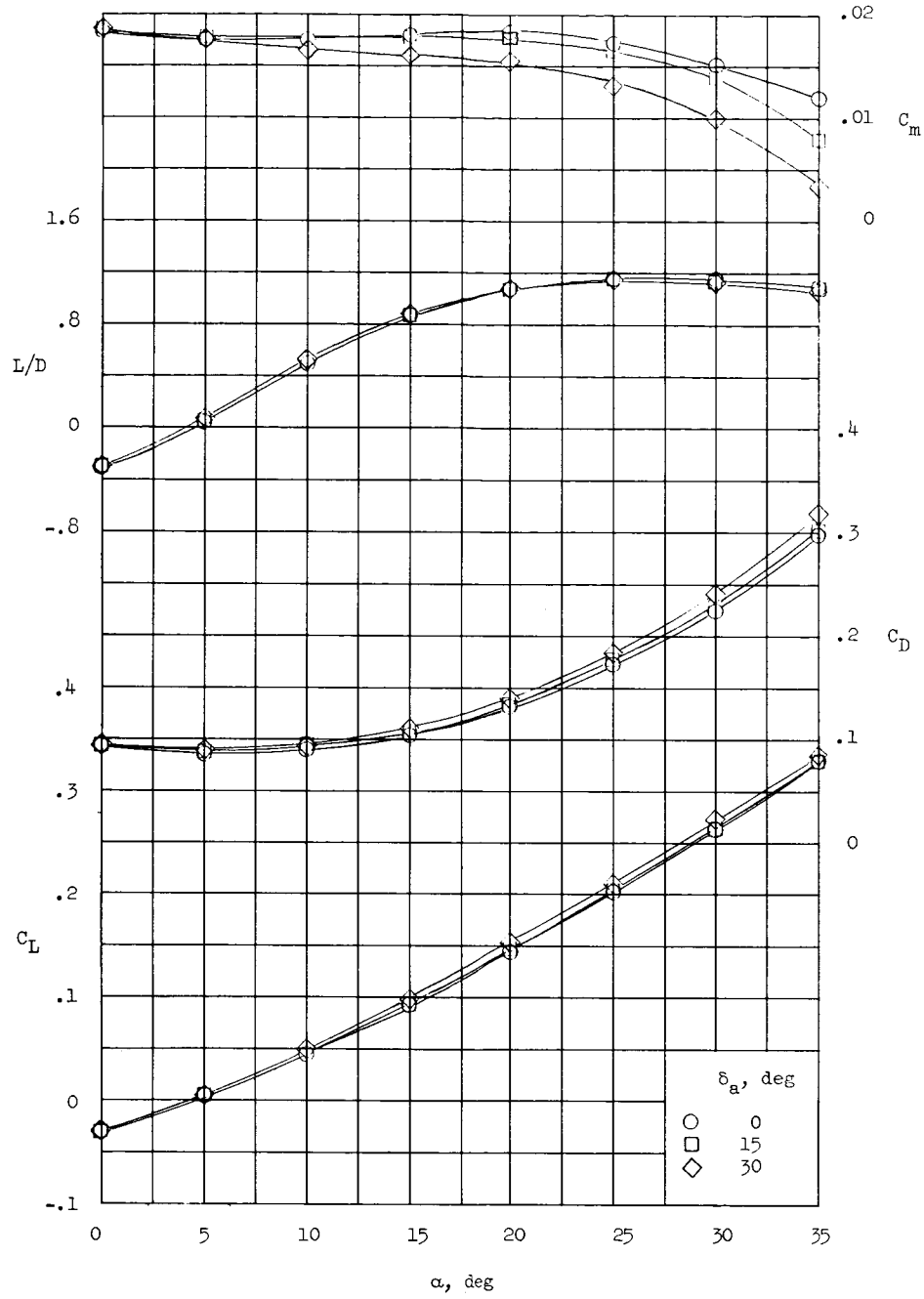

(b) $\delta_e = 15^0$.

Figure 12.- Continued.

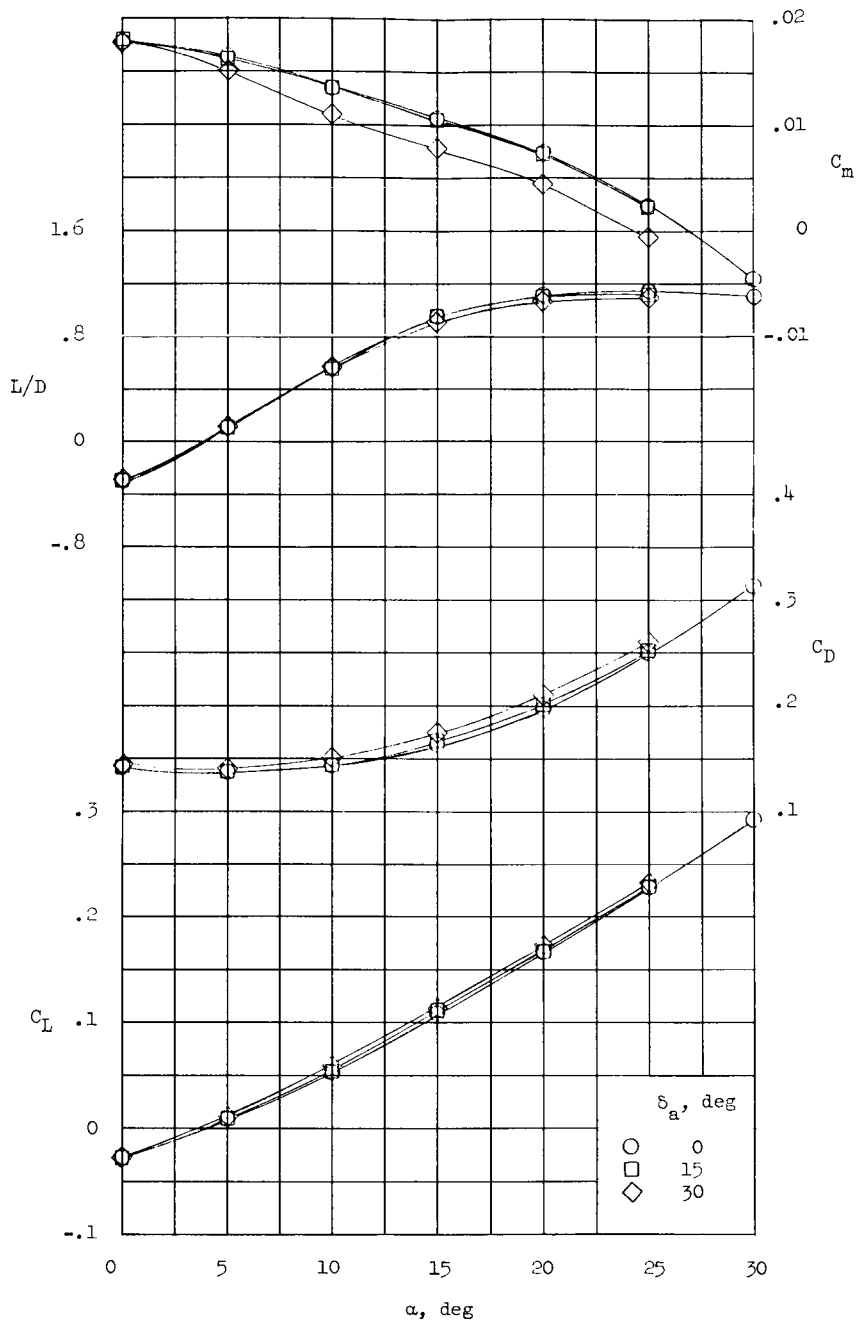

(c) $\delta_e = 30^0$.

Figure 12.- Concluded.

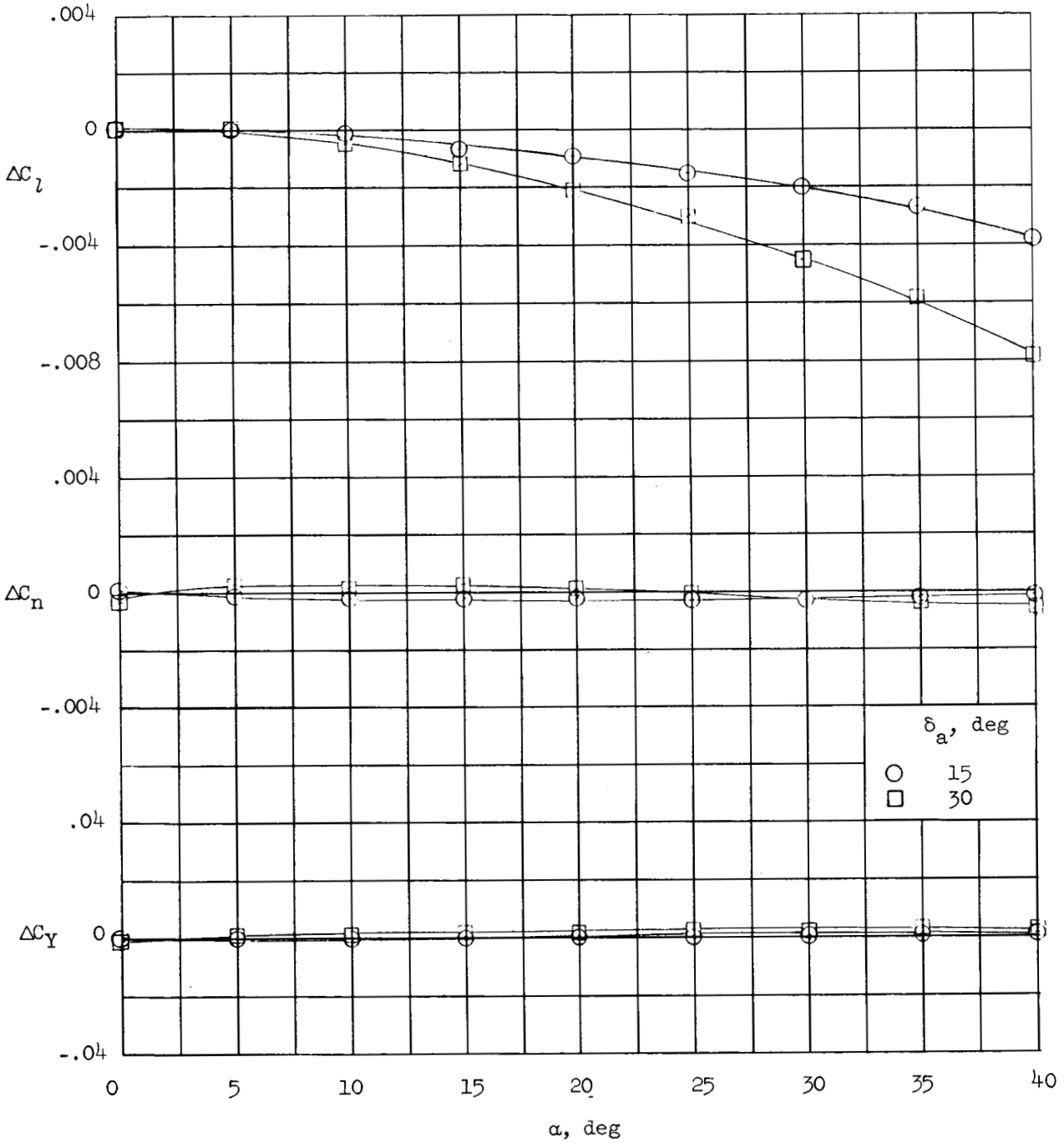

(a) $\delta_e = 0^0$.

Figure 13.- Lateral control characteristics of configuration with tip fin I_4 and center fin E_2.

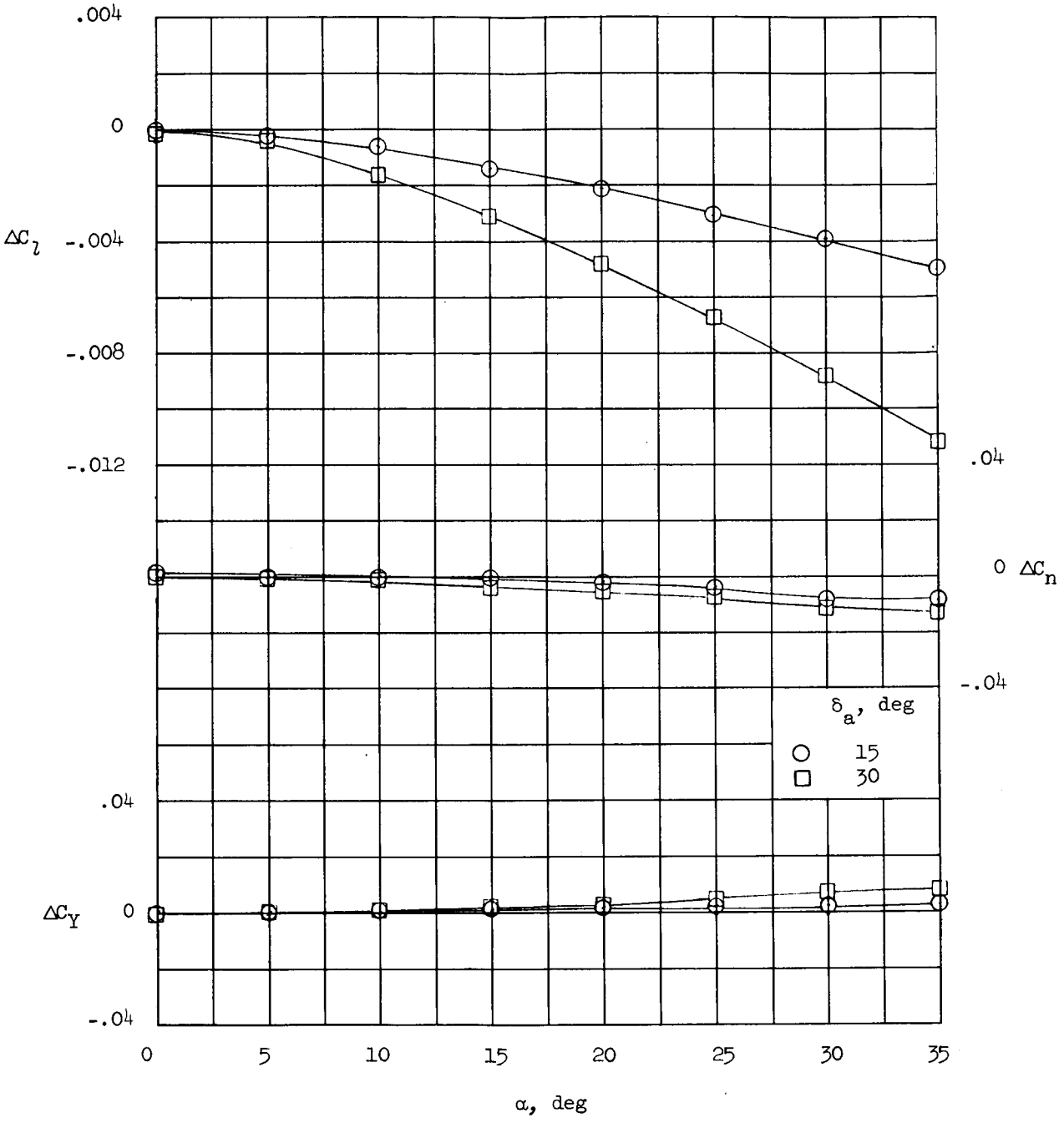

(b) $\delta_e = 15^0$.

Figure 13.- Continued.

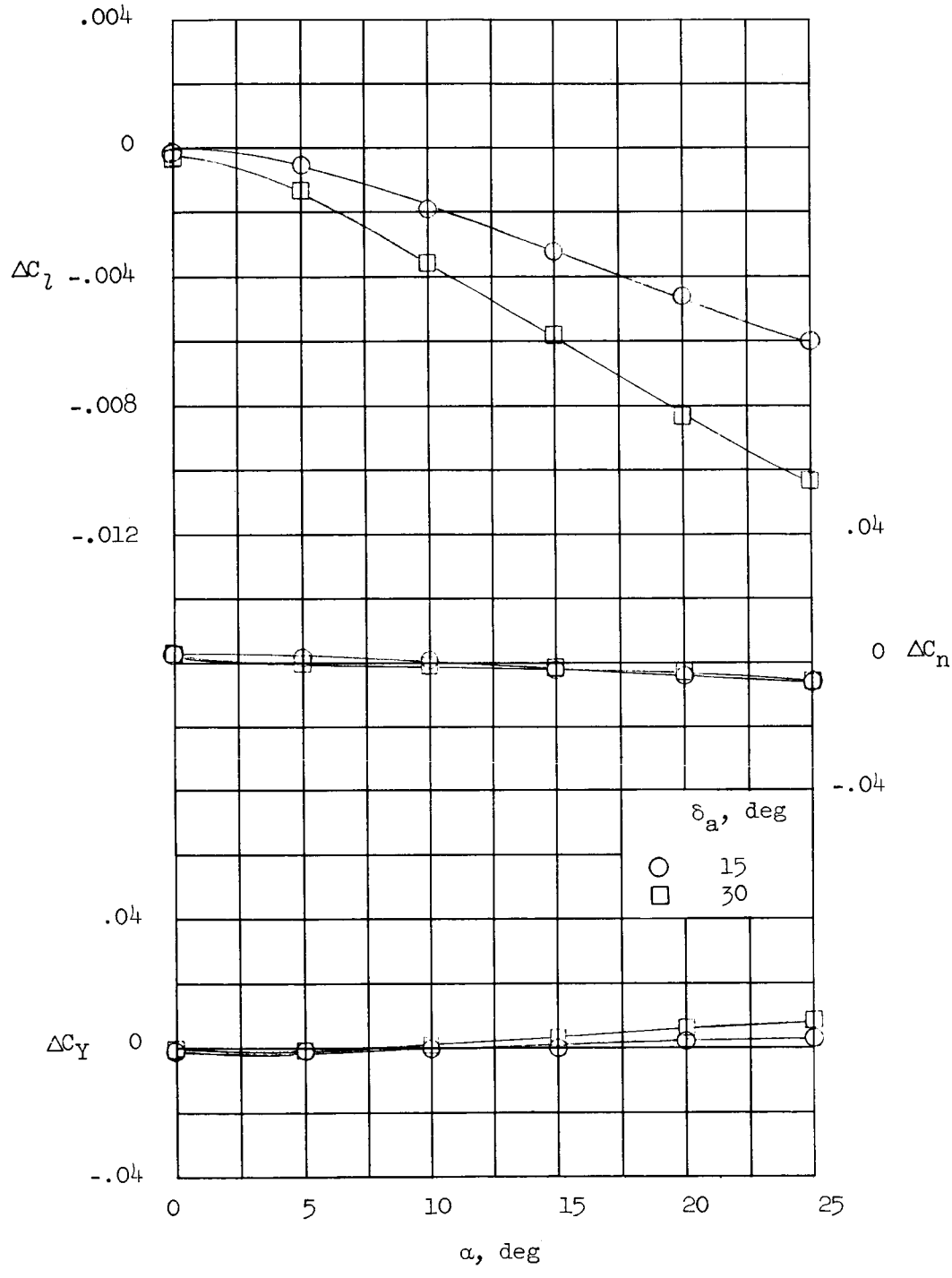

(c) $\delta_e = 30^0$.

Figure 13.- Concluded.

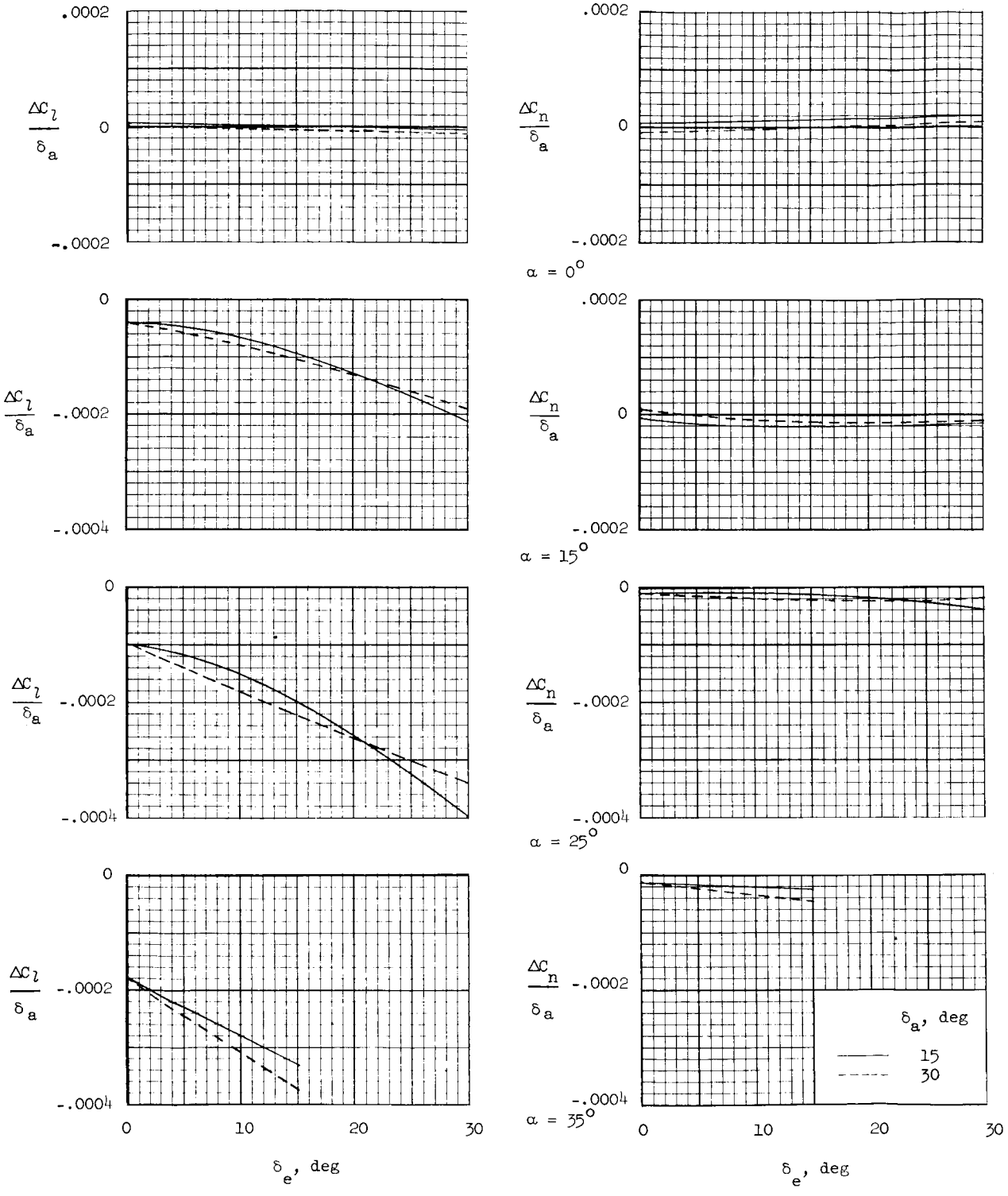

Figure 14.- Effect of elevon deflection angle on lateral control characteristics.

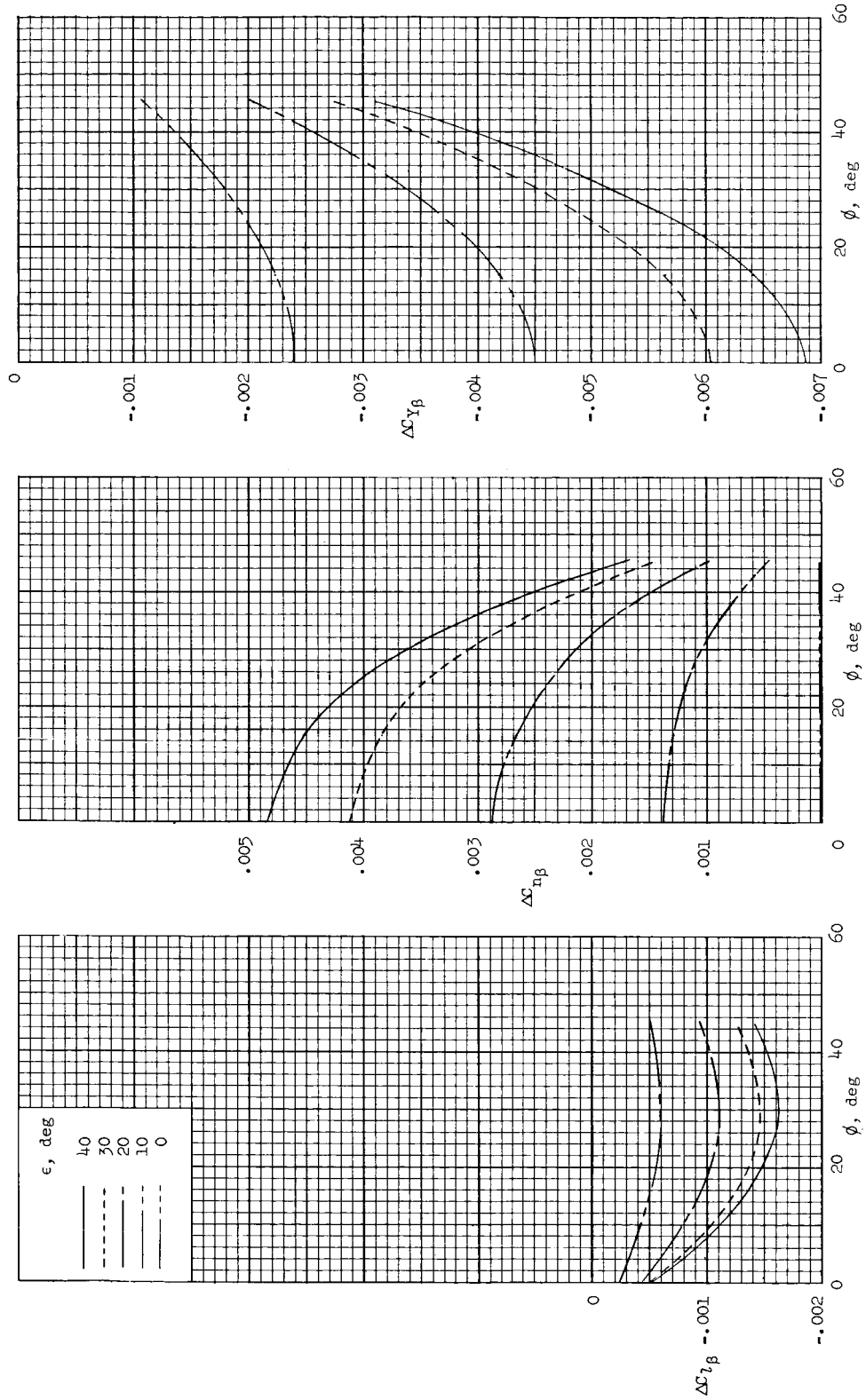

(a) $\alpha = 0°$.

Figure 15.- Newtonian calculations showing effect of toe-in angle and roll-out angle on incremental lateral stability parameters.

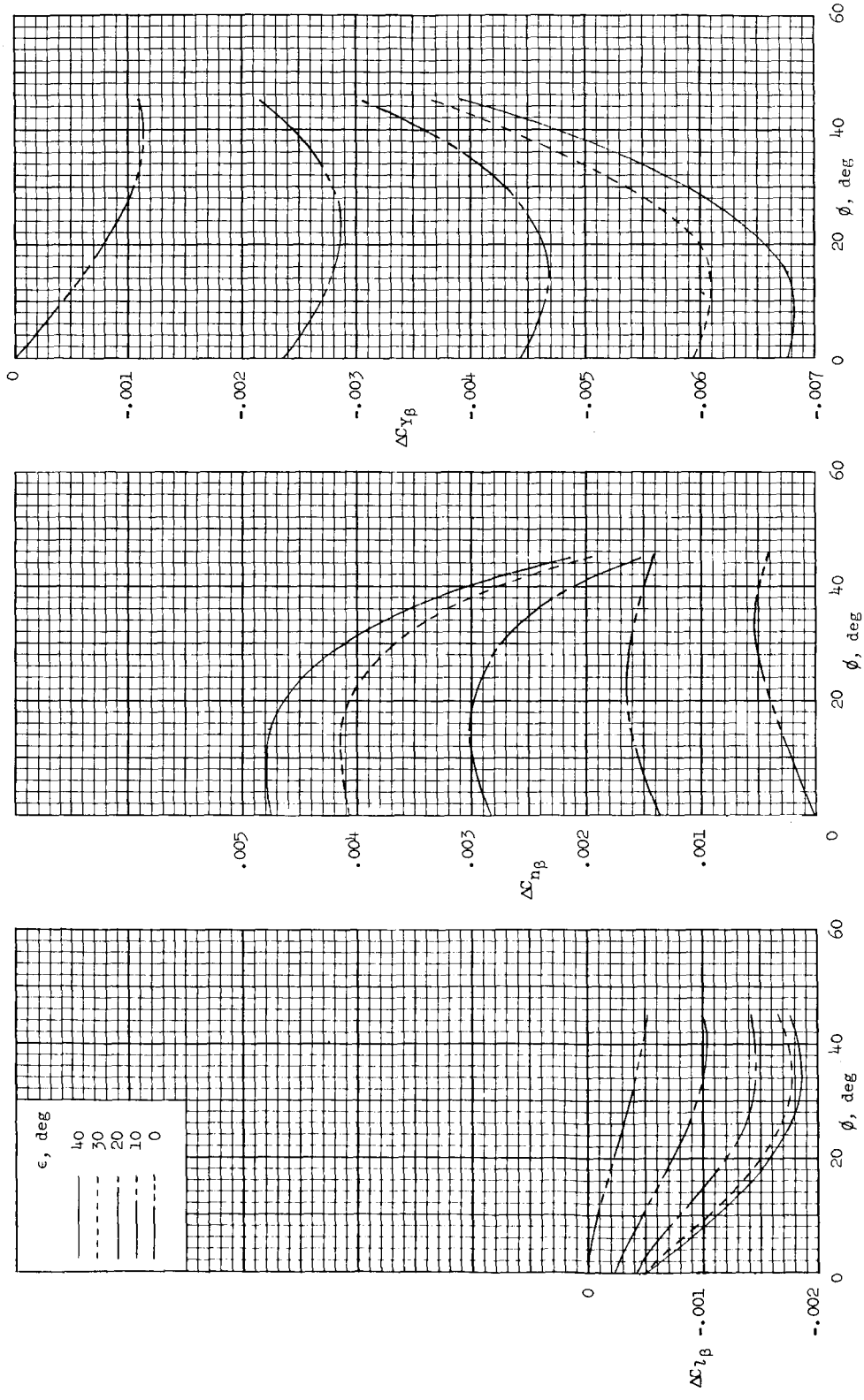

(b) $\alpha = 10^0$.

Figure 15.- Continued.

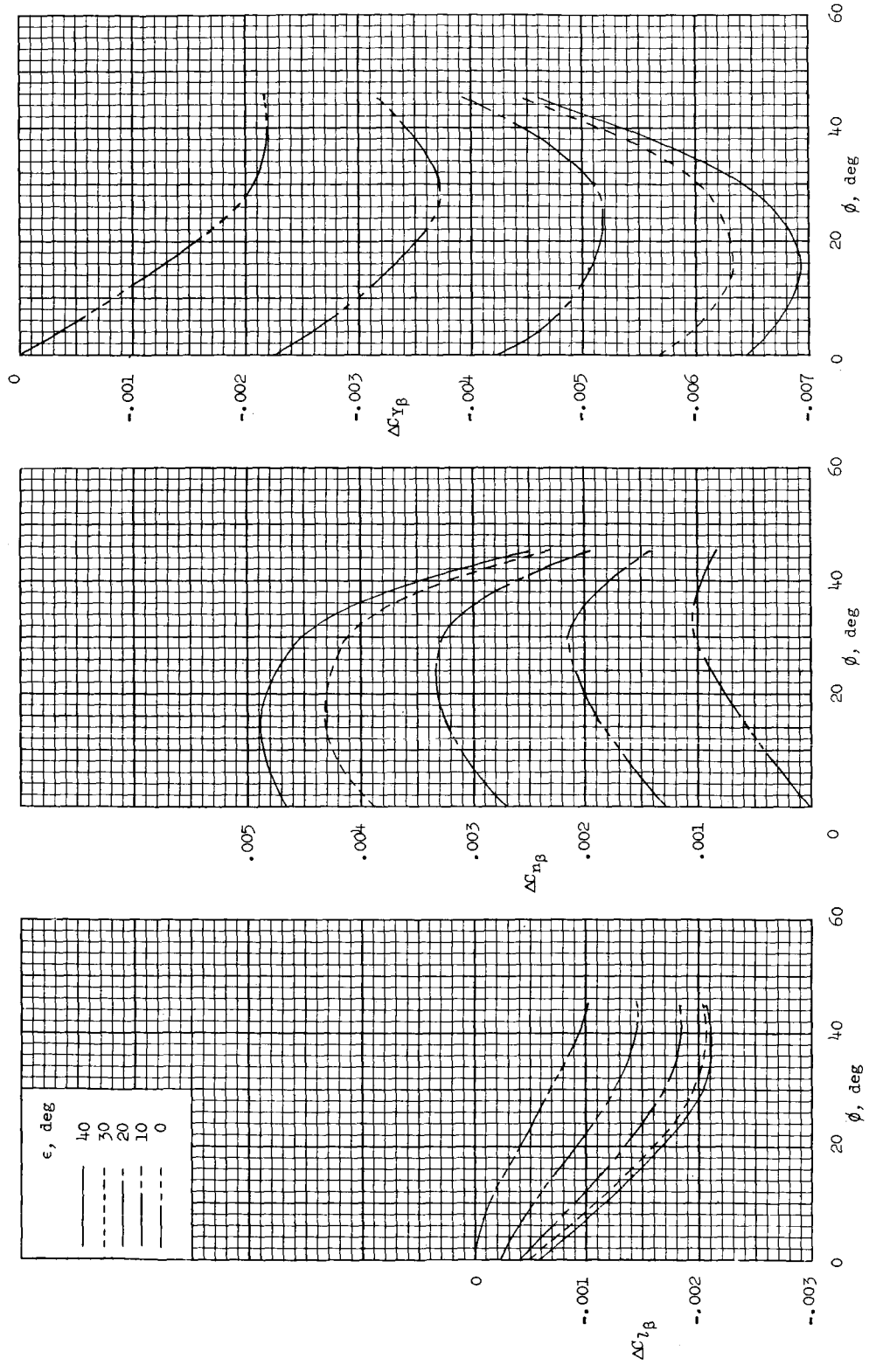

(c) $\alpha = 20^0$.

Figure 15.- Continued.

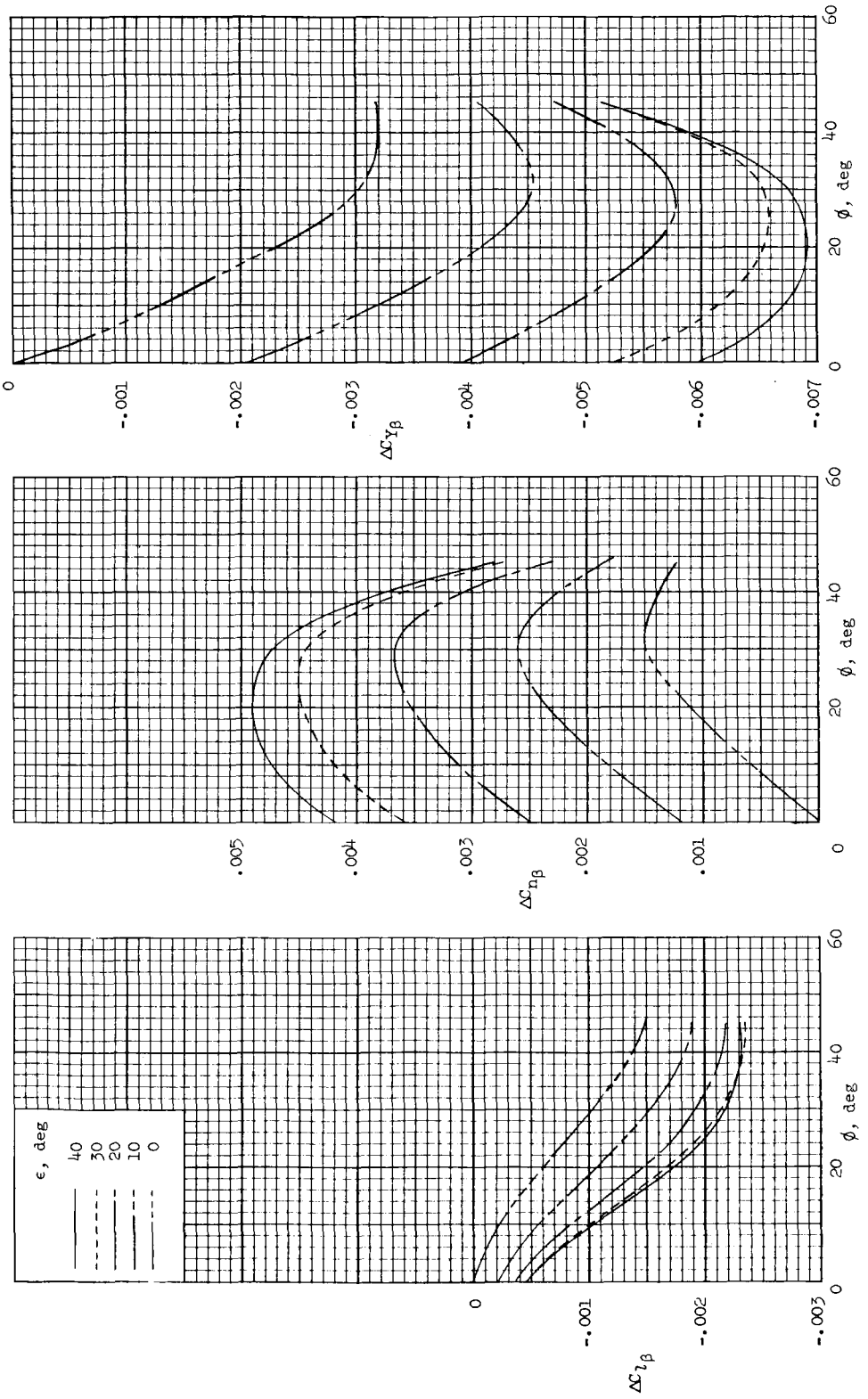

(d) $\alpha = 30^0$.

Figure 15.- Continued.

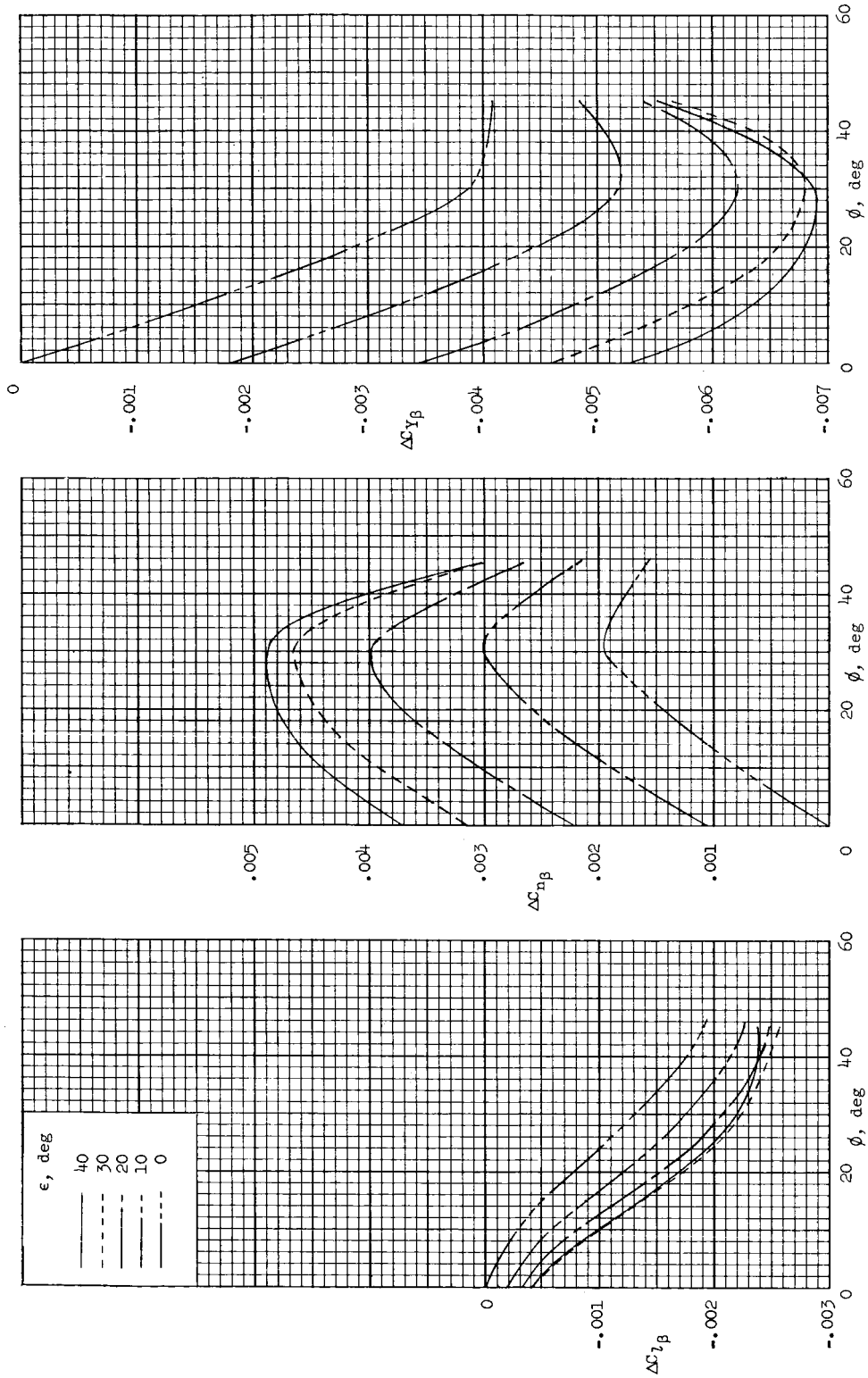

(e) $\alpha = 40^0$.

Figure 15.- Continued.

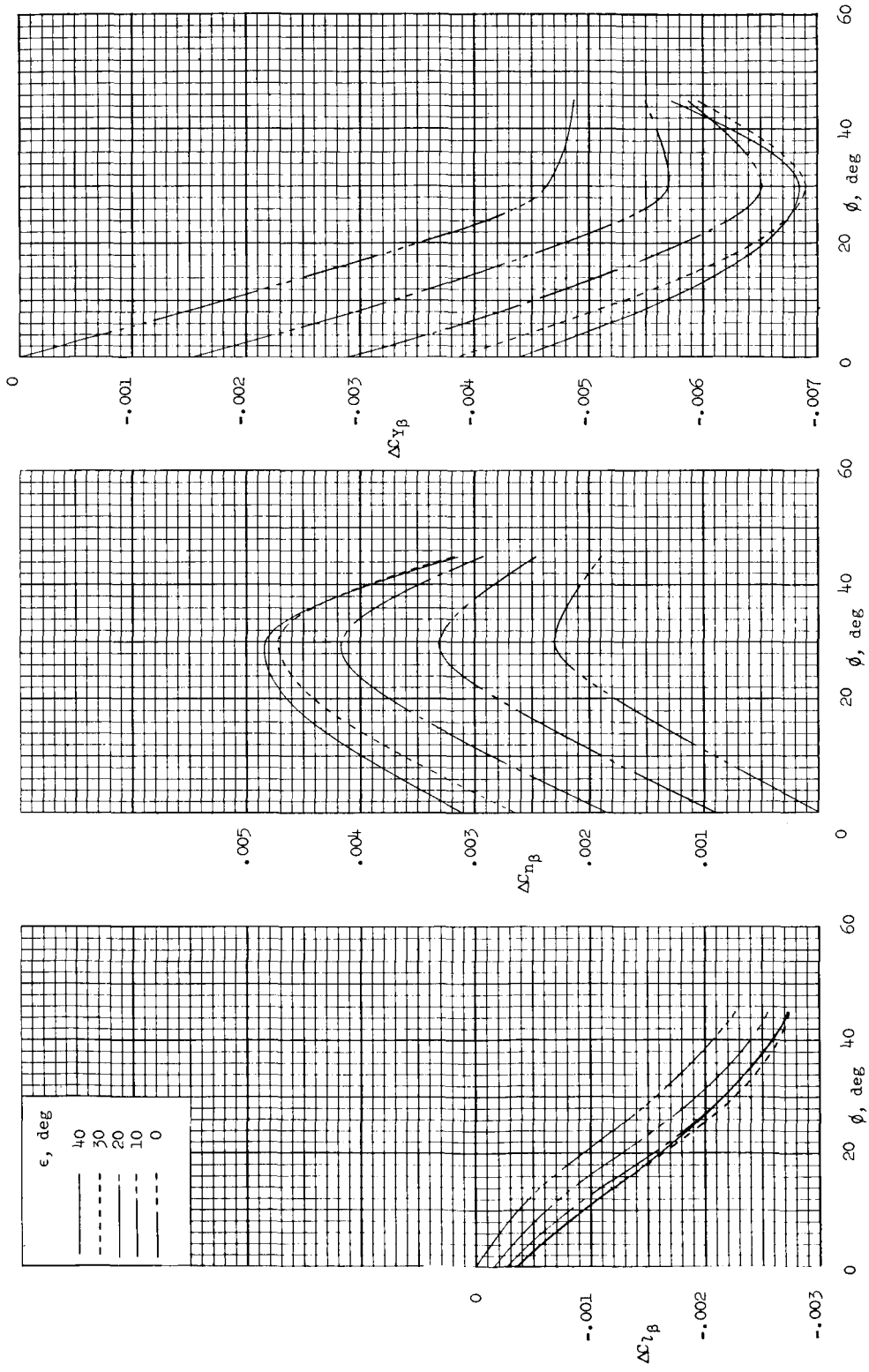

(f) $\alpha = 50^0$.

Figure 15.- Continued.

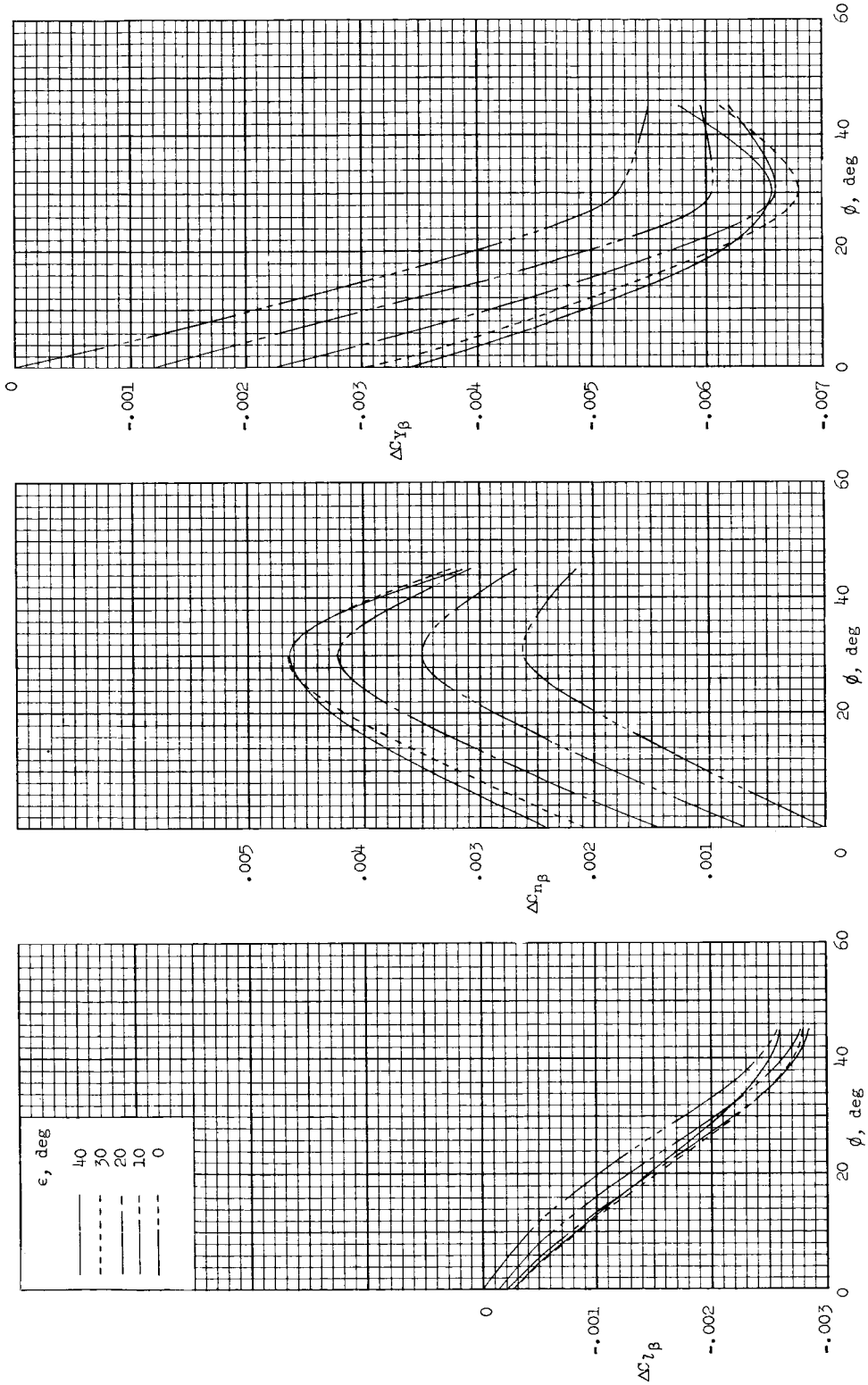

(g) $\alpha = 60^0$.

Figure 15.- Continued.

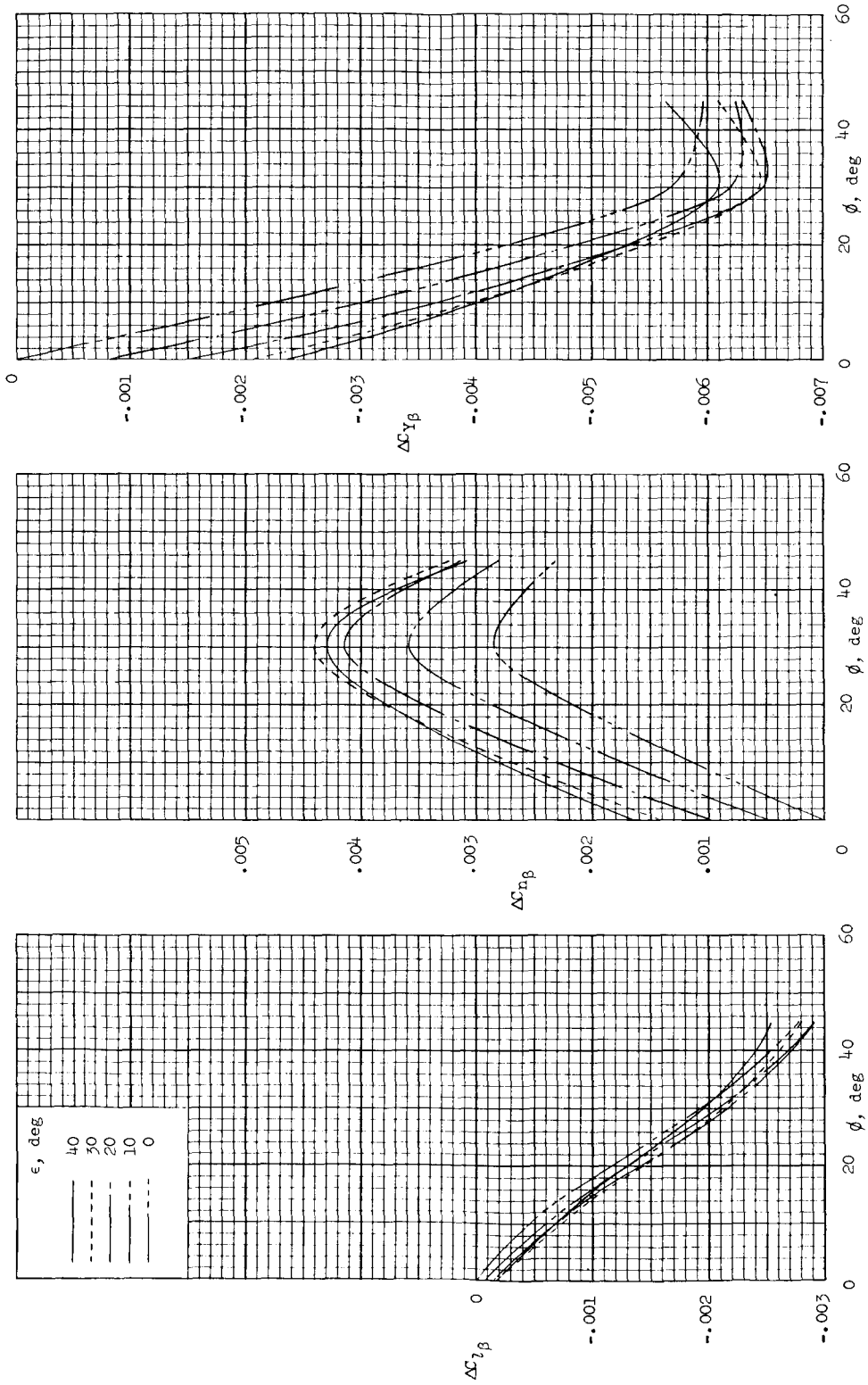

(h) $\alpha = 70^0$.

Figure 15.- Concluded.

NASA-Langley, 1965 L-4378

"The aeronautical and space activities of the United States shall be conducted so as to contribute . . . to the expansion of human knowledge of phenomena in the atmosphere and space. The Administration shall provide for the widest practicable and appropriate dissemination of information concerning its activities and the results thereof."

—NATIONAL AERONAUTICS AND SPACE ACT OF 1958

NASA SCIENTIFIC AND TECHNICAL PUBLICATIONS

TECHNICAL REPORTS: Scientific and technical information considered important, complete, and a lasting contribution to existing knowledge.

TECHNICAL NOTES: Information less broad in scope but nevertheless of importance as a contribution to existing knowledge.

TECHNICAL MEMORANDUMS: Information receiving limited distribution because of preliminary data, security classification, or other reasons.

CONTRACTOR REPORTS: Technical information generated in connection with a NASA contract or grant and released under NASA auspices.

TECHNICAL TRANSLATIONS: Information published in a foreign language considered to merit NASA distribution in English.

TECHNICAL REPRINTS: Information derived from NASA activities and initially published in the form of journal articles.

SPECIAL PUBLICATIONS: Information derived from or of value to NASA activities but not necessarily reporting the results of individual NASA-programmed scientific efforts. Publications include conference proceedings, monographs, data compilations, handbooks, sourcebooks, and special bibliographies.

Details on the availability of these publications may be obtained from:

SCIENTIFIC AND TECHNICAL INFORMATION DIVISION

NATIONAL AERONAUTICS AND SPACE ADMINISTRATION

Washington, D.C. 20546